

A Novel Method to Constrain Tidal Quality Factor from A Non-synchronized Exoplanetary System

TAKATO TOKUNO ^{1,2} AKIHIKO FUKUI ^{3,4} AND TAKERU K. SUZUKI ^{1,2,3}

¹ *Department of Astronomy, School of Science, The University of Tokyo, 7-3-1 Hongo, Bunkyo-ku, Tokyo 113-0033, Japan*

² *School of Arts & Sciences, The University of Tokyo, 3-8-1 Komaba, Meguro, Tokyo 153-8902, Japan*

³ *Komaba Institute for Science, The University of Tokyo, 3-8-1 Komaba, Meguro, Tokyo 153-8902, Japan*

⁴ *Instituto de Astrofísica de Canarias, Vía Láctea s/n, E-38205 La Laguna, Tenerife, Spain*

ABSTRACT

We propose a novel method to constrain the tidal quality factor, Q' , from an observed non-synchronized star-planet system consisting of a slowly rotating low-mass star and a close-in Jovian planet, taking into account the co-evolution of stellar spin and planetary orbit due to the tidal interaction and the magnetic braking. On the basis of dynamical system theory, the track of the co-evolution of angular momentum from the fast rotator regime for such a system exhibits the existence of a forbidden region in the $\Omega_{\text{orb}} - \Omega_{\text{spin}}$ plane, where Ω_{spin} and Ω_{orb} denote the angular velocity of the stellar spin and planetary orbit, respectively. The forbidden region is determined primarily by the strength of the tidal interaction. By comparing $(\Omega_{\text{orb}}, \Omega_{\text{spin}})$ of a single star-planet system to the forbidden region, we can constrain the tidal quality factor regardless of the evolutionary history of the system. The application of this method to the star-planet system, NGTS-10 – NGTS-10 b, gives $Q' \gtrsim 10^8$, leading to an tight upper bound on the tidal torque. Since this cannot be explained by previous theoretical predictions for non-synchronized star-planet systems, our result requires mechanisms that suppress the tidal interaction in such systems.

Keywords: Exoplanet systems (484) — Exoplanet tides (497) — Star-planet interactions (2177) — Low mass stars (2050) — Hot Jupiters (753) — Analytical mathematics (38)

1. INTRODUCTION

Thanks to recent space telescope missions such as *Kepler* (Borucki et al. 2010) and TESS (Ricker et al. 2014) and to the follow-up missions using ground telescopes, a large number ($\gtrsim 5500$) of exoplanets have been detected. A significant fraction of them is orbiting a low-mass main-sequence star that possesses a convective envelope, similarly to our solar-system planets. High-quality observational data enable us to obtain precise stellar, planetary, and orbital parameters of numerous star-planet systems (e.g., NASA Exoplanet Archive; Akeson et al. 2013) and to reveal unexpectedly great diversity of star-planet systems (see, e.g., Winn & Fabrycky 2015; Jontof-Hutter 2019).

One of the representative examples that are not common in the Solar system is close-in Jovian planets. The firstly discovered exoplanet orbiting a solar-like star was

such a “hot Jupiter”, 51 Pegasi b (Mayor & Queloz 1995), and since then, hot Jupiters have been observed at a high frequency, whereas there is a caveat that hot Jupiters are preferentially identified by the radial velocity and planetary transit techniques. They are commonly considered to have formed beyond the ice line and migrated inward to their current positions (see, e.g., Dawson & Johnson 2018; Fortney et al. 2021). The migration of planets is induced by interactions with the central star, disk, and other planets/companions (see, e.g., Perryman 2018, Section 10.10 and 10.11).

In particular, the tidal interaction between a low-mass star and a close-in Jovian exoplanet is one of the key mechanisms of the star-planet interaction. The tidal dissipation in the stellar interior, which we focus on hereafter, plays an important role in the last phase of planetary migration. Specifically, when the stellar spin is slow, the tidal interaction transports the orbital angular momentum (AM) to the stellar spin, reducing the semi-major axis and spin-orbit inclination angle of the planetary orbit (Darwin 1880; Zahn 1977; Hut 1981; Barker

& Ogilvie 2009). While the orbital decay is confirmed for only one system, WASP-12 b (e.g., Yee et al. 2020), low-inclination trends in close-in companions orbiting around a low-mass star are acquired statistically (Winn et al. 2010; Albrecht et al. 2012, 2022). Also, the AM transport causes a spin-up of the host star, and this tendency is observationally obtained by the statistical examination (Tejada Arevalo et al. 2021). In addition to the spin-up effect, the tidal interaction has also attracted attention in terms of stellar magnetism because it may increase stellar magnetic activity (Cuntz et al. 2000). However, despite the importance, quantitatively consistent treatment of the efficiency of the tidal interaction has yet to be established because of both theoretical and observational difficulties.

First, the tidal interaction is a complex problem that is composed of multiple nonlinear processes (e.g., Ogilvie 2014, see also Section 2.1.3), making self-consistent quantitative discussion a challenging task. Additionally, the low-mass stars also lose their AM through the magnetic braking effect (Weber & Davis 1967; Kawaler 1988; Matt et al. 2012; Shoda et al. 2020). When considering both the magnetic braking effect and tidal interaction, the co-evolution of AM is expected to exhibit complicated behaviors (Dobbs-Dixon et al. 2004; Barker & Ogilvie 2009; Damiani & Lanza 2015; Gallet & Delorme 2019; Benbakoura et al. 2019).

Second, it is extremely difficult to directly constrain the theoretically obtained tidal strength. In order to do so, we have to know the evolutionary history of star-planet systems, at least the age of systems and the initial distribution of planets (e.g., Penev et al. 2014, 2018). While the stellar age, which roughly corresponds to the age of the system, is basically determined by isochrones of stellar model grids (e.g., Baraffe et al. 2015; Choi et al. 2016), Tayar et al. (2022) showed that the derived age includes systematic uncertainty of tens of percent and that, furthermore, model dependence cannot be ignored. In addition to that, recent observations by ALMA reveal diverse nature of protoplanetary disks and their evolution, suggesting that it is a herculean task to pin down initial distributions of planets in different systems (see, e.g., Drążkowska et al. 2023; Miotello et al. 2023, for detail). It is difficult to remove the indecisiveness of results due to these uncertainties.

The main purpose of this paper is to investigate the method to restrict the efficiency of tidal interaction without facing the above uncertainties. Then, we focus on the non-synchronized system composed of a slowly-rotating low-mass star and a close-in Jovian planet in order to simplify the physical picture. Also, considering the differential equations governing the AM co-evolution

from a mathematical viewpoint of the dynamical system, we propose a novel method to impose a constraint on the efficiency of tidal interaction. A great advantage of our method is that we require only minimal assumptions about the model of tidal interaction and about the age and initial condition of the system, respectively.

The outline of this paper is as follows. In Section 2, we first describe the formulation of AM co-evolution and propose a novel method to constrain the tidal interaction using the dynamical system concept. After the brief introduction of observational data (Section 3), we show the main obtained by applying our method to observations (Section 4). Discussions and conclusions are presented in Sections 5 and 6, respectively.

2. METHOD

In this section, we describe the methodology of our approach. We first introduce our framework (Section 2.1). By giving some assumptions, we formulate to track the AM co-evolution of the star-planet system. Next, we explain how to constrain the efficiency of tidal interactions using the mathematical concept of the dynamical system (Section 2.2). Finally, we describe the specific procedures for application to observations in Section 2.3.

Before starting the analysis, we make a remark about our target system. We set the two-body system formed by a low-mass main-sequence star and a close-in Jovian planet orbiting it. We consider the time evolution after the zero-age main sequence (ZAMS), which is defined here as the stage when the stellar spin is fastest as a result of the contraction (e.g., Bouvier et al. 1997; Gallet & Bouvier 2013). The typical lifetime of protoplanetary disks is $\lesssim 10$ Myr (Ribas et al. 2015; Kunitomo et al. 2020), which is shorter than the duration of the pre-main sequence phase of low-mass stars before reaching the ZAMS. Therefore, we ignore the effect of the migration driven by disk-planet interaction.

We also assume that both stellar and planetary properties, such as mass and radius, except for the rotation are constant with time for simplification. In fact, this assumption is not strictly correct. A low-mass main-sequence star generally expands and brightens with evolution. Detailed stellar evolution calculations shows that the lower the stellar mass is, the smaller the variation rate of the stellar parameter is. On the other hand, while planetary mass and radius may decrease through atmospheric escape (e.g., Owen 2019), it is considered that the Jovian planets can maintain their envelope (e.g., Kurokawa & Nakamoto 2014). On the basis of the above discussions, this assumption is reasonable for the system that consists of a low-mass central star and a massive gaseous planet. In this paper, we consider a K or M-

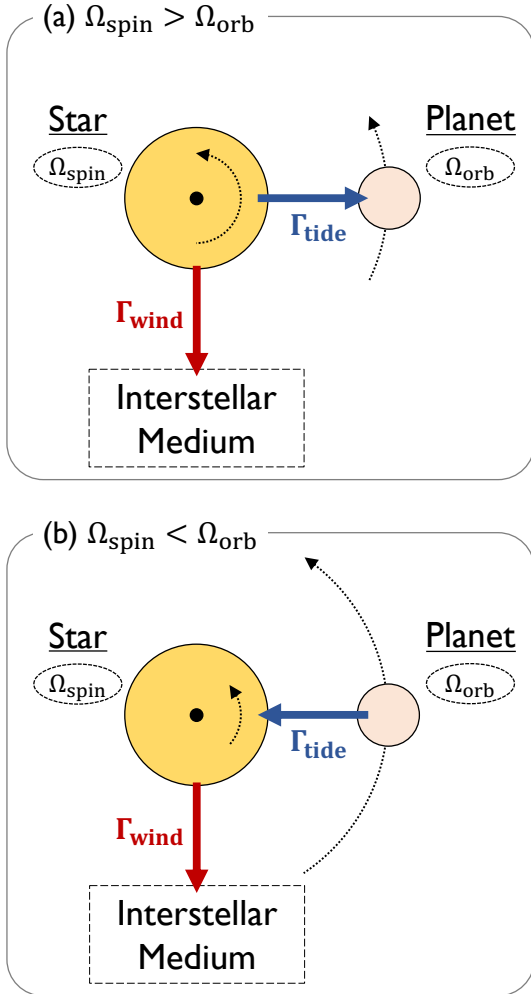


Figure 1. Schematic picture of AM co-evolution in a star-planet system. The red and blue arrows represent the AM transport through the magnetic braking and the tidal interaction, respectively. In (a), the planet is orbiting outside the co-rotation radius. Since $\Omega_{\text{spin}} > \Omega_{\text{orb}}$ in this case, the AM of the stellar rotation is transferred to the orbital AM by the tidal interaction. In (b), the planet is inside the co-rotation radius and $\Omega_{\text{spin}} < \Omega_{\text{orb}}$; the orbital AM is transferred to the spin AM by the tidal interaction. In both cases, the magnetic braking always removes the AM of the system.

type star, $M_s \leq 0.8 M_\odot$, and a gas-giant planet with $M_p \geq 0.5 M_J$, where M_s , M_p , M_\odot and M_J represent the stellar mass, planetary mass, Solar mass and Jovian mass, respectively. Quantitative verification of the errors caused by this treatment is presented in Section 5.1. We note that, hereafter, the suffixes “s”, “p”, “ \odot ”, and “J” represent the variables of star, planet, the Sun and the Jupiter, respectively.

2.1. Framework for AM evolution

2.1.1. Basic equations

The time evolution of AM is driven by the tidal interaction and magnetic braking. While the central star loses the spin AM by the magnetic braking, the tidal interaction, which is driven by an internal force, exchanges the spin AM of the star,

$$J = I_s \Omega_{\text{spin}}, \quad (1)$$

and the orbital AM,

$$h = M_s M_p G^{2/3} (M_s + M_p)^{-1/3} \Omega_{\text{orb}}^{-1/3}, \quad (2)$$

where I_s , Ω_{spin} , Ω_{orb} , and G denote the stellar moment of inertia, the angular velocity of stellar spin, the orbital angular velocity, and the gravitational constant, respectively. In equation (1) we are assuming that the stellar spin is rigid¹. In equation (2) both star and planet are assumed to be rotating around the center of the two-body masses with circular orbits (Jackson et al. 2008, see also Section 3 for our target selection). It should be noted that h is mostly carried by the AM of the planetary orbit in the case with $M_p \ll M_s$.

In addition to the abovementioned simplifications, we assume that the orbital rotational axis is aligned with the stellar spin axis (Winn et al. 2010; Albrecht et al. 2012, 2022; Morgan et al. 2024) and that the spin of the planet is synchronized to the orbit. The second assumption is justified because the timescale of synchronization (~ 1 Myr for a close-in Jovian planet; Guillot et al. 1996) is much shorter than the lifetime of the system and because the AM of planetary spin is negligible compared to the total AM.

The time evolution of J and h is described by the following equations (cf. Benbakoura et al. 2019):

$$\frac{dJ}{dt} = \Gamma_{\text{tide}} - \Gamma_{\text{wind}} \quad (3)$$

and

$$\frac{dh}{dt} = -\Gamma_{\text{tide}}, \quad (4)$$

where $\Gamma_{\text{wind}} (> 0)$ and Γ_{tide} mean the torques through the magnetic braking (“wind torque”, hereafter) and tidal interaction (“tidal torque”, hereafter), respectively. In this formulation, we set the sign of Γ_{tide} to plus (minus) when the planet orbit the star inside (outside) the co-rotation radius. Figure 1, a schematic picture of our system governed by equations (3) and (4), shows the behavior of both wind and tidal torques.

¹ In fact, it has been observed that there is differential rotation in the Sun (e.g., Schou et al. 1998) and some low-mass stars (e.g., Benomar et al. 2018), but we can make a similar discussion if we regard Ω_{spin} as the averaged angular velocity.

Substituting equations (1) and (2) into equations (3) and (4), we obtain

$$\frac{d\Omega_{\text{spin}}}{dt} = \frac{\Gamma_{\text{tide}} - \Gamma_{\text{wind}}}{I_s} \quad (5)$$

and

$$\frac{d\Omega_{\text{orb}}}{dt} = \frac{3\Omega_{\text{orb}}^{4/3}\Gamma_{\text{tide}}}{\mu[G(M_s + M_p)]^{2/3}}, \quad (6)$$

where $\mu = (M_s M_p)/(M_s + M_p)$ is the reduced mass. We note that I_s is assumed to be constant with time, and thus, we neglect the time variation term.

2.1.2. Formulation of wind torque

Skumanich (1972) discovered a simple relation between stellar rotation and age, t , via

$$\Omega_{\text{spin}} \propto t^{1/p}, \quad (7)$$

where the power-law index takes a standard value of $p \sim 2$. Later observations confirm this trend (Barnes 2007; Angus et al. 2015). Without tidal interaction ($\Gamma_{\text{tide}} = 0$), we obtain $\Gamma_{\text{wind}} \propto \Omega_{\text{spin}}^{p+1}$ from equations (5) and (7). This power-law relation is supported by one-dimensional magnetohydrodynamical (1D MHD) numerical simulations for Alfvén wave-driven magnetorotating winds conducted by Shoda et al. (2020).

However, recent observations suggest complicated behavior that does not obey equations (8): wind torque is considered to be saturated for fast rotators (El-Badry et al. 2022; Gossage et al. 2023; Belloni et al. 2024) and weakened for slow rotators (van Saders et al. 2016; Hall et al. 2021). The detail of these effects is described in Appendix A. In this formulation, we include the former effect but ignore the latter because our observational samples are non-slow rotators that are unaffected by this effect (see Section 5.1)

The saturated wind torque in the fast rotator regime is deviated from $\Gamma_{\text{wind}} \propto \Omega_{\text{spin}}^{p+1}$ and can be scaled as $\Gamma_{\text{wind}} \propto \Omega_{\text{spin}}$ (e.g., Matt et al. 2012, see also Appendix A). Then, we obtain the wind torque formula as

$$\Gamma_{\text{wind}} = \begin{cases} \alpha_{\text{mb}} \left(\frac{\Omega_{\text{spin}}/2\pi}{0.05 \text{ d}^{-1}} \right)^{p+1} & \text{for } \Omega \leq \Omega_{\text{sat}} \\ \alpha_{\text{mb}} \left(\frac{\Omega_{\text{sat}}/2\pi}{0.05 \text{ d}^{-1}} \right)^p \left(\frac{\Omega_{\text{spin}}/2\pi}{0.05 \text{ d}^{-1}} \right) & \text{for } \Omega > \Omega_{\text{sat}} \end{cases}. \quad (8)$$

Ω_{sat} is the critical angular velocity that divides the saturated and unsaturated regimes. We adopt Ω_{sat} for the

Rossby number, $\text{Ro} = 0.1$ (see Appendix A), which corresponds to the threshold for the saturated magnetic activity of low-mass stars (e.g., Wright et al. 2011; Matt et al. 2015; See et al. 2019). α_{mb} is the reference value in $\Omega_{\text{spin}}/2\pi = 0.05 \text{ d}^{-1}$, when the Skumanich's law is satisfied regardless of stellar mass² (see Figure 8). We assume that α_{mb} , which generally depends on stellar properties, is determined solely by stellar mass, $\alpha_{\text{mb}} = \alpha_{\text{mb}}(M_s)$, and is constant over the evolution in our analysis (see the beginning of Section 2).

We adopt the wind torque expression of equation (8) and set $p = 2$ for simplicity. This simplification enables us to derive α_{mb} by comparing the spin-down model with the observed spin rate in the cluster members whose age is estimated (see Appendix B).

2.1.3. Formulation of tidal torque

In a traditional framework (e.g., Goldreich & Soter 1966), the efficiency of tidal interaction is characterized by the modified (dimensionless) quality factor Q' , which is inversely proportional to the phase lag between the tidal potential and the tidal bulge divided by the tidal Love number (see Ogilvie 2014). The tidal interaction is formulated using Q' as (see, e.g., Murray & Dermott 1999; Benbakoura et al. 2019)

$$\Gamma_{\text{tide}} = \text{sign}(\Omega_{\text{orb}} - \Omega_{\text{spin}}) \frac{R_s^5 \Omega_{\text{orb}}^4 \mu^2}{GM_s^2} \left(\frac{9}{4Q'} \right). \quad (9)$$

Here, R_s is the stellar radius. We note that $\text{sign}(\Omega_{\text{orb}} - \Omega_{\text{spin}})$ controls the behavior of Γ_{tide} (cf. Figure 1), which is discussed in the text after the equations (3) and (4).

Determining the specific form of Q' remains a complex problem. Here, we assume that Q' is approximated by the power of the tidal frequency, $\omega_{\text{tide}} \equiv 2|\Omega_{\text{orb}} - \Omega_{\text{spin}}|$, with a floor value:

$$Q' = \max \left[Q'_0 \left(\frac{\omega_{\text{tide}}/2\pi}{2 \text{ d}^{-1}} \right)^{-q}, Q'_{\text{min}} \right], \quad (10)$$

where Q'_0 means the reference value for $\omega_{\text{tide}}/2\pi = 2 \text{ d}^{-1}$ and q is the power-law index. We consider that Q'_0 depends on stellar parameters and then constant in our analysis. $Q'_{\text{min}} (> 0)$ is a minimum value of Q' , which corresponds to the maximum efficiency of the tidal interaction.

The power-law relation in equation (10) comes from theoretical suggestion by previous papers dealing with

² Previous empirical relations adopt the solar spin rate ($\sim 0.035 \text{ d}^{-1}$) as the reference value (cf. Gossage et al. 2023). However, recent papers (Metcalfe et al. 2022, 2023; Saunders et al. 2024) suggest that the solar spin rate is so slow that the magnetic braking is weakened (see text and appendix A).

the tide in the radiative zone of low-mass stars induced by internal gravity wave (Zahn 1975; Goodman & Dickson 1998; Barker & Ogilvie 2010; Essick & Weinberg 2016; Ma & Fuller 2021). We note that, while the equilibrium/non-wave-like tide (Zahn 1966; Zahn & Bouchet 1989; Remus et al. 2012; Mathis et al. 2016) and the dynamical tide in a convective zone induced by inertial wave (Ogilvie & Lin 2007; Ogilvie 2013; Mathis 2015) are generally suggested as notable mechanisms, Barker (2020) claims that they are subdominant for slowly rotating solar-type stars, which are the main target of this paper (see Sections 2.3). However, even when limited to the tide in the radiative zone, the detailed mechanism is not still well understood (Appendix C) and there are large uncertainties in Q'_0 and q . Then, we treat them as the free parameters to constrain Q' .

The setting of the lower bound of Q'_{\min} in equation (10) is required to avoid the divergence of $\Gamma_{\text{tide}}(\propto 1/Q')$ for $Q' = 0$ (equation 9) at the co-rotation radius where $\omega_{\text{tide}} = 0$ for a negative value of q (cf. Penev et al. 2018). A non-zero Q'_{\min} is also reinforced from an observational point of view because there have been already a number of non-synchronized or eccentric close-in Jovian planets identified (e.g., Matsumura et al. 2008, 2010); these observations contradict a spurious enhancement in Γ_{tide} at the co-rotation radius because it makes close-in planets synchronized and circularized. We note that the divergence of Q' at $\omega_{\text{tide}} = 0$ does not cause problematic behavior for positive q because it simply gives $\Gamma_{\text{tide}}(\propto 1/Q') = 0$.

The presence of a lower bound of Q' is also required owing to the fact that a variation in the transit timing has not been detected for close-in planets (e.g., Ivshina & Winn 2022; Adams et al. 2024), except for WASP-12 b (Yee et al. 2020; Turner et al. 2021; Wong et al. 2022). We note that the host star WASP-12 has $\sim 1.4 M_{\odot}$ (Collins et al. 2017), which is larger than the low-mass stars we focus on.

For the WASP-12 – WASP-12 b system, Q' is estimated to be about 1.5×10^5 (Wong et al. 2022). For lower-mass stars, there is any confident detection of orbital decay by the transit-time variation, which implies larger Q' (Patra et al. 2020; Maciejewski et al. 2018, 2020, 2022; Mannaday et al. 2022; Rosário et al. 2022; Harre et al. 2023). Throughout this paper, we set a conservative value of $Q'_{\min} = 1 \times 10^5$. We note that results in the following sections are hardly affected by a choice of Q'_{\min} , provided $10^4 \lesssim Q'_{\min} \lesssim 10^6$ (see Section 2.3).

2.2. Trajectories and forbidden region in phase space

We can track the AM co-evolution of the star-planet system from equations (5) (6), (8), (9), and (10). We

Table 1. Model parameters to determine the trajectory in $\Omega_{\text{orb}} - \Omega_{\text{spin}}$ plane from equations (5) (6), (8), (9), and (10).

Given Parameter		
Symbol	Description	Equation
M_s	Stellar mass	(6) (9)
R_s	Stellar radius	(9)
I_s	Stellar moment of inertia	(5)
M_p	Planetary mass	(6) (9)
α_{mb}	Reference value of Γ_{wind} for 20-day spin period ($\Omega_{\text{spin}}/2\pi = 0.05 \text{ d}^{-1}$)	(8)
Free Parameter		
Symbol	Description	Equation
Q'_0	Tidal Q' factor for 0.5-day tidal period ($\omega_{\text{tide}}/2\pi = 2 \text{ d}^{-1}$)	(10)
q	Power-law index of Q'	(10)

Table 2. The tendency of the AM co-evolution. A sign in the cell indicates that of a formula written at the top of the column.

Stage	Input		Output	
	$\Omega_{\text{spin}} - \Omega_{\text{orb}}$	$\Gamma_{\text{tide}} - \Gamma_{\text{wind}}$	$d\Omega_{\text{spin}}/dt$	$d\Omega_{\text{orb}}/dt$
1	+	–	–	–
2	–	–	–	+
3	–	+	+	+

describe the characteristic physical properties in the phase space of $(\Omega_{\text{orb}}, \Omega_{\text{spin}})$ by using a system composed of a low-mass K-type star with $M_s = 0.70 M_{\odot}$ and $R_s = 0.70 R_{\odot}$ and a Jovian planet with $M_p = 1.0 M_J$ and $R_p = 1.0 R_J$, where R_p is the planetary radius³.

We set the initial spin rate of the central star to the range of $\Omega_{\text{spin,init}}/2\pi \gtrsim 0.1 \text{ d}^{-1}$, referring to the observed spin rate of stars in ZAMS (e.g., Gallet & Bouvier 2013, 2015, see also Figure 9). We presume that the initial position of the planet is sufficiently outside the Roche radius because otherwise such a system cannot survive for a long time. This condition corresponds to the initial orbital angular velocity $\Omega_{\text{orb,init}}/2\pi \lesssim 2 \text{ d}^{-1}$. Except for these two presumptions, there are no restrictions regarding the initial conditions to cover a diversity of planetary systems.

We calculate the evolution of $(\Omega_{\text{orb}}, \Omega_{\text{spin}})$ for standard values of the wind torque parameter, $\alpha_{\text{mb}} = 1.5 \times$

³ R_p is used not for tracking the trajectory but for the calculation of the Roche radius. In this paper, we adopt $2.46 R_p (M_s/M_p)^{1/3}$ as the formulation of Roche radius (cf. Collier Cameron & Jardine 2018).

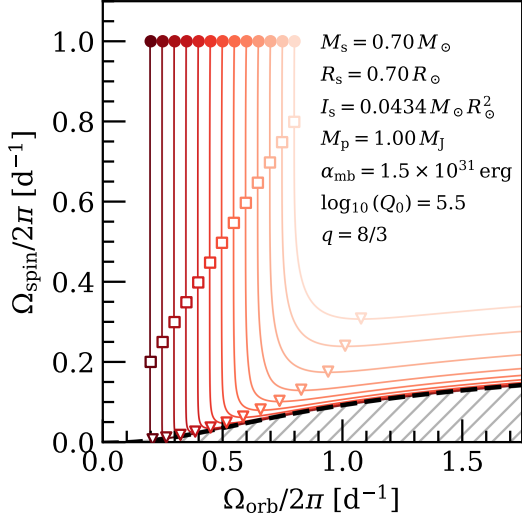


Figure 2. Trajectories (colored lines) in phase space of $(\Omega_{\text{orb}}, \Omega_{\text{spin}})$ derived from equations (5) (6), (8), (9), and (10). We also show the forbidden region (the gray hatched region) and its boundary (the black dashed line), which is obtained by the solution of equation (11) that passes the origin. The colors of the lines correspond to the initial values of orbital angular velocity $\Omega_{\text{orb,init}}$ with the initial condition marked with filled circles, whereas we set the initial spin rate to a constant value, $\Omega_{\text{spin,init}}/2\pi = 1 \text{ d}^{-1}$. The open squares (triangles) represent the transition from stage 1 to stage 2 (from stage 2 to stage 3) in Table 2. We note that other astrophysical settings that are adopted here are written in the upper-right corner (see also texts in Section 2.2). It should be mentioned that the boundary is called “unstable manifold” in text.

10^{31} erg , reproducing the observed spin-down trend (see Appendix B) and the tidal parameters, $q = 8/3$ and $Q'_0 = 10^{5.5}$, adopted from the wave-breaking model (Barker & Ogilvie 2010; Barker 2020, see Appendix C), whereas the qualitative behavior described below is preserved regardless of the choice of these parameters. We also assume that the stellar properties, including the moment of inertia, $I_s = 0.0435 M_\odot R_\odot^2$, determined from the stellar evolution code MESA (r12778; Paxton et al. 2011, 2013, 2015, 2018, 2019, see also Appendix D), are unchanged with time.

Figure 2 shows trajectories in the phase space (the red lines) for the initial stellar spin, $\Omega_{\text{spin,init}}/2\pi = 1.0 \text{ d}^{-1}$. The trajectories can be separated into three evolutionary stages, listed in Table 2. First, in the stage 1, the stellar spin is decelerated both through the wind torque and the tidal torque because $\Omega_{\text{spin}} > \Omega_{\text{orb}}$ (see also Figure 1(a)). While Ω_{orb} also decreases in the stage 1, it is not explicitly visible in Figure 2 because $\Gamma_{\text{wind}} \gg \Gamma_{\text{tide}}$. Next, in the stage 2, the tidal torque begins to transport AM from the planet to the star as $\Omega_{\text{spin}} < \Omega_{\text{orb}}$ (see

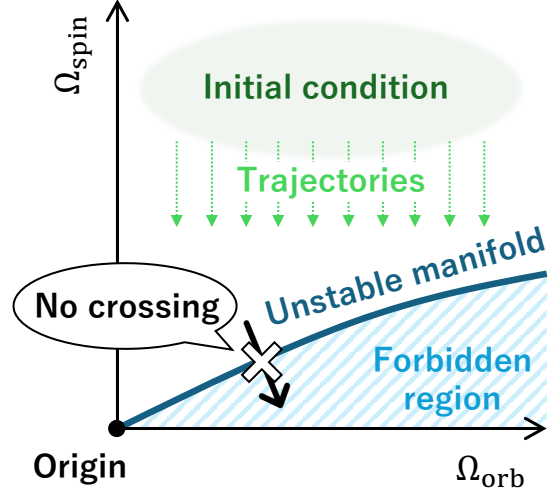


Figure 3. Schematic pictures showing the reason for the existence of the forbidden area. The dark green shaded region and light green dotted arrows correspond to the initial condition and trajectories, respectively, which are determined by astrophysical conditions. The dark blue line represents the unstable manifold, which is one of the solutions of equation (11) passing through the origin. Because a mathematical argument shows that the unstable manifold can not be intersected (the black arrow with comment), we can show the existence of the forbidden region (the light blue hatched region).

also Figure 1(b)), while a star continues to spin down because $\Gamma_{\text{wind}} > \Gamma_{\text{tide}}$. Finally, in the stage 3, the tidal torque overcomes the wind torque, and then both stellar spin and planetary revolution are accelerated. This tendency is summarized in Table 3. We note that the observational targets we utilize to constrain the tidal torque are the systems including slowly rotating stars in the stages 2 and 3 listed in Table 2.

A characteristic feature of these trajectories is that they never cross a particular curve (the black dashed line). That is to say, there is the forbidden area (the hatched area) in the phase space of $(\Omega_{\text{orb}}, \Omega_{\text{spin}})$. The existence and property of the forbidden area are explained by combining astrophysical conditions and mathematical properties of the dynamical system theory. We proceed with the discussion without mathematical rigorous proofs used here, while a brief introduction is presented in Appendix E (see, e.g., Arnold 1992; Hsieh & Sibuya 1999, for more detail).

Under the assumption that the stellar parameters are constant, the right-hand side of the governing differential equations (equations 5 and 6) does not explicitly depend on the independent variable, t . Such a system of differential equations is called an ‘autonomous system’ in the dynamical system theory. When we consider the equations as a two-dimensional autonomous system, the

trajectories are obtained as the solution of the tangent of equations (5) and (6) (see Appendix E):

$$\frac{d\Omega_{\text{spin}}}{d\Omega_{\text{orb}}} = \left(1 - \frac{\Gamma_{\text{wind}}}{\Gamma_{\text{tide}}}\right) \frac{\mu[G(M_s + M_p)]^{2/3}}{3\Omega_{\text{orb}}^{4/3} I_s}. \quad (11)$$

Namely, the trajectories on the $\Omega_{\text{orb}} - \Omega_{\text{spin}}$ plane are not explicitly dependent on t . Therefore, given the stellar parameters and one passing point, we can track the trajectory through that point. As an important property derived from this, it shows that one trajectory does not intersect with another one (see Appendix E).

Here, we focus on the trajectories passing through the origin, which are unphysical solutions. One trajectory is a trivial solution satisfying $\Omega_{\text{orb}} = 0$, which is going downward along the Ω_{spin} axis to the origin. The other one, what is noteworthy here, is a non-trivial solution, which appears as a trajectory away from the origin on the phase space (the black dashed line in Figure 11)⁴. In a dynamical system, the latter (former) is called an “unstable manifold” (“stable manifold”)⁵. The unstable manifold has two additional characteristic properties besides passing through the origin: 1. the unstable manifold is not intersected by any other solution; 2. both Ω_{spin} and Ω_{orb} are physically required to have non-negative values. According to them, we show that all physically possible trajectories belong only to one of the two subspaces: above or below the unstable manifold. The schematic picture summarizing the discussion is shown in Figure 3.

The astrophysically reasonable conditions mentioned earlier place the initial position of $(\Omega_{\text{orb,init}}, \Omega_{\text{spin,init}})$ above the unstable manifold in the phase space, whereas the opposite case will be discussed in Section 5.1. Thereby, the trajectories for such system can not enter below the unstable manifold, and therefore the forbidden area appears in the phase space of $(\Omega_{\text{orb}}, \Omega_{\text{spin}})$.

2.3. Procedure to constrain tidal quality factor

The trajectories in the $(\Omega_{\text{orb}}, \Omega_{\text{spin}})$ space depend on the efficiency parameters of the tidal interaction and the magnetic braking in addition to the stellar and planetary parameters (Table 1). Similarly, the solution of the unstable manifold, and accordingly the area occupied by the forbidden region, is dependent on these parameters. Therefore, by comparing observed $(\Omega_{\text{orb}}, \Omega_{\text{spin}})$ of star-planet systems, we can constrain them; if observed $(\Omega_{\text{orb}}, \Omega_{\text{spin}})$ was located in the forbidden region,

⁴ When a lower bound of Q'_{min} is set in equation (10), such a solution always exist, even if q is negative.

⁵ The origin corresponds to the saddle equilibrium point in the dynamical system.

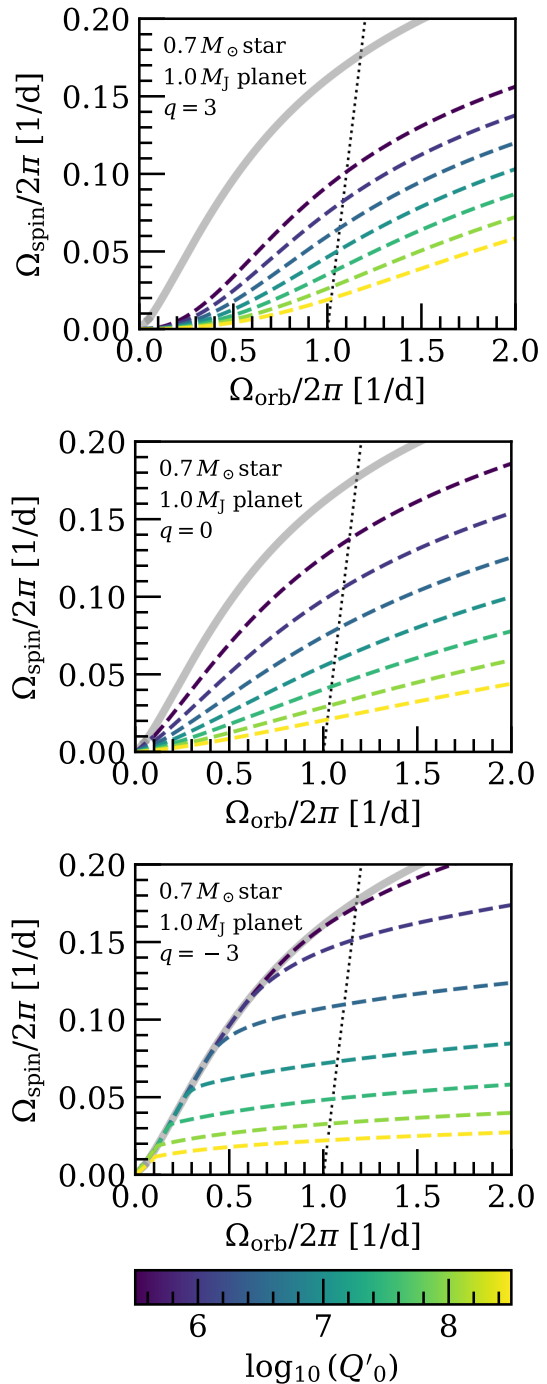


Figure 4. The dependence of unstable manifold (color-dotted lines) for a $0.7 M_{\odot}$ star + $1 M_J$ planet system on Q'_0 when $q = 3$ (top panel), $q = 0$ (middle panel) and $q = -3$ (bottom panel). The colors of the lines correspond to Q'_0 shown in the bottom color-bar. The black dotted lines represent $\omega_{\text{tide}}/2\pi = 2 \text{ d}^{-1}$. We also show the unstable manifold for $Q'_0 = Q_{\text{min}}$ and $q = 0$ by the gray solid line.

it would require modification of the input value of the parameters. In this paper, we fix the wind torque pa-

parameter to the standard value of $\alpha_{\text{mb}} = 1.5 \times 10^{31}$ erg (Section 2.2 and Appendix B), and give constraints on the tidal quality factor, Q' .

Figure 4 shows unstable manifolds for various Q'_0 and q . They show that smaller Q'_0 , which causes stronger tidal interaction, results in steeper slopes of the unstable manifold and greater areas of the forbidden region in the phase space. This is because the right-hand side of equation (11) (> 0 for the unstable-manifold solutions) has a negative correlation with Q'_0 for any q . The dependence on q , which looks slightly more complex, can also be understood from the dependence on tidal strength; namely, stronger tidal torque gives a steeper slope of the unstable manifold. In the negative (positive) q cases presented in the bottom (top) panel, the tidal torque is stronger for smaller (larger) ω_{tide} (see equations 9 and 10), which corresponds to the upper left (lower right) side of the panel. If one compares the slopes of unstable manifolds for a given Q'_0 but with different q values, smaller q cases give steeper (shallower) slopes in the smaller (larger) ω_{tide} side.

In Figure 4 we also plot the unstable manifold for $Q'_0 = Q'_{\text{min}}$ and $q = 0$, giving constant $Q' = Q'_{\text{min}}$ (gray solid line). The forbidden area shaped by this manifold is larger than any other forbidden area formed with $Q'_0 > Q'_{\text{min}}$ for arbitrary q .

Let us suppose a situation in which an observed $(\Omega_{\text{orb}}, \Omega_{\text{spin}})$ in a star-planet system is located in the forbidden region for an arbitrary guessed set of (q, Q'_0) . This discrepancy indicates that the initial guess of Q'_0 was too small for this q value; we can derive $Q'_{0,\text{lim}} (> Q'_0)$ that gives the unstable manifold passing exactly through the observed $(\Omega_{\text{orb}}, \Omega_{\text{spin}})$. The same procedure can be done for different q values so that we can derive the lower bound, $Q'_{0,\text{lim}}(q)$, as a function of q . We note that, as long as the observed point is located inside the maximum forbidden region derived from $Q'_0 = Q'_{\text{min}}$ and $q = 0$ (the gray solid line in Figure 4), the existence of $Q'_{0,\text{lim}}(q) \geq Q'_{\text{min}}$ is guaranteed.

The novelty of our method is that the unstable manifold does not depend on time and the initial condition of the system. If one can fix the five “given parameters” listed in Table 1, a single set of observed $(\Omega_{\text{orb}}, \Omega_{\text{spin}})$ in a star-planet system at any evolutionary stage can constrain the tidal quality factor in the two-dimensional (q, Q'_0) parameter space. Although this study does not take into account finite eccentricity, e , and spin-orbit inclination, i , our method can be applied without error as long as e and i are (nearly) zero at the time of observation, even if these took finite values during the evolution before the observation (see the discussion in Section 5.3).

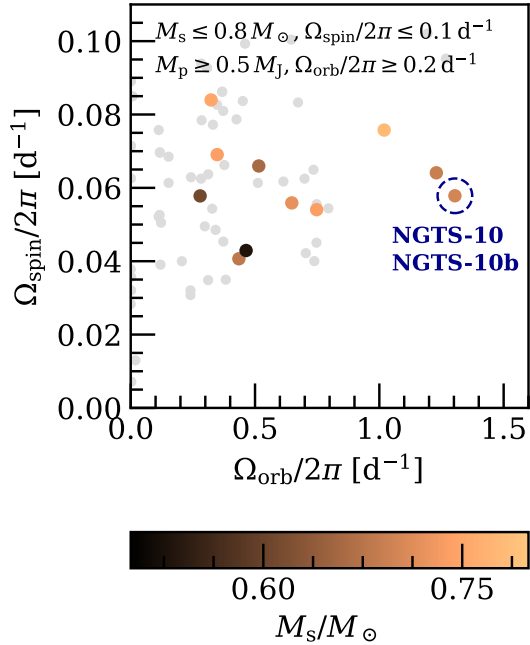


Figure 5. Observed values (circle symbols) of the orbital angular velocity of planet Ω_{orb} (abscissa) and the stellar spin rate Ω_{spin} (ordinate), which are obtained from NASA Exoplanet Archive. The large colored symbols show the selected samples, where the selection criteria for these samples are described in Section 3. The color of the marker refers to the stellar mass M_s normalized by the Solar mass, which is decoded on the bottom color-bar. The small gray symbols represent the systems with Jovian planets with $M_p \geq 0.5 M_J$ that do not satisfy the criteria. Our target system, NGTS-10 – NGTS-10 b, is highlighted.

From an astrophysical point of view, our method gives an upper bound on the tidal torque from a close-in Jovian planet orbiting around a slowly rotating low-mass star. If such a system is observed in the lower right side of the phase space, it will provide a stringent constraint on the tidal torque because sufficiently weak tidal interaction is required to avoid the stellar spin-up by the transfer of AM from the planet. Since this methodology is simple and straightforward, our method is applicable to general tidal torque recipes (e.g., Barker 2020) besides the parametrization in equation (10).

3. TARGET SELECTION

In this section, we briefly introduce the observational data we utilize. Our targets are non-synchronized systems consisting of a slowly rotating low-mass star and a close-in gaseous planet with a circular orbit because their observation can be directly compared with our model (Section 2). Then, from the list of observed plane-

Table 3. Parameters we adopt for the target system, NGTS-10 – NGTS-10 b. We also show the source of them.

Object: NGTS-10 – NGTS-10 b		
Parameters (star)	Values	Source
M_s	$0.696 \pm 0.040 M_\odot$	*1
R_s	$0.697 \pm 0.036 R_\odot$	*1
T_{eff}	$4600 \pm 150 \text{ K}$	*1
I_s	$0.0435 M_\odot R_\odot^2$	*2
α_{mb}	$1.5 \times 10^{31} \text{ erg}$	*3
$\Omega_{\text{spin}}/2\pi$	$0.0578 \pm 0.0000 \text{ d}^{-1}$	*1
Parameters (planet)	Values	Source
M_p	$2.16 \pm 0.10 M_J$	*1
R_p	$1.21 \pm 0.11 R_J$	*1
$\Omega_{\text{orb}}/2\pi$	$1.3040 \pm 0.000 \text{ d}^{-1}$	*1

NOTE—*1 The literature (McCormac et al. 2020), *2 The MESA calculation (see Appendix D), *3 Fitting to the observed spin rates (see Appendix B)

tary systems of NASA Exoplanet Archive⁶ (Akeson et al. 2013), we extract the stars satisfying the following conditions: $M_s \leq 0.8 M_\odot$, $M_p \geq 0.5 M_J$, $0.02 \leq \Omega_{\text{spin}}/2\pi \leq 0.1 \text{ d}^{-1}$, $\Omega_{\text{orb}}/2\pi \geq 0.2 \text{ d}^{-1}$, and $e \leq 0.1$. Figure 5 shows the plot of the extracted samples (colored symbols) in the phase space of $(\Omega_{\text{orb}}, \Omega_{\text{spin}})$ among other samples satisfying $M_p \geq 0.5 M_J$ (small gray symbols). We can confirm that no data is distributed in the lower-right region of $\Omega_{\text{orb}} - \Omega_{\text{spin}}$ plane; the shape of the empty region looks exactly like a forbidden region in Figures 3 and 4.

On the basis of the discussion in Sections 2.2 and 2.3, the sample with the largest $\Omega_{\text{orb}}/\Omega_{\text{spin}}$ gives the most severe restrictions. Then, we focus on NGTS-10 – NGTS-10 b (McCormac et al. 2020), which was first detected in the Next Generation Transit Survey (NGTS; Wheatley et al. 2018), as the suitable target in this paper⁷. Table 3 shows the pre-determined parameters to constrain the tidal quality factor (see Section 2.3). Most of the stellar and planetary parameters originate from McCormac et al. (2020), who derived them by multiple techniques including transit photometry, radial velocity measurements, and SED fitting. We ignore observational errors of these quantities. The stellar moment of inertia I_s is calculated by the gyration radius

⁶ <https://exoplanetarchive.ipac.caltech.edu/>

⁷ Figure 5 shows that WASP-43 system, which is the closest point to the NGTS-10 system in the figure, is also suitable. However, Davoudi et al. (2021) report later that the stellar spin is twice faster than the plotted value (from Esposito et al. 2017), which does not satisfy the condition in the statement. Therefore, we eliminate it from the target.

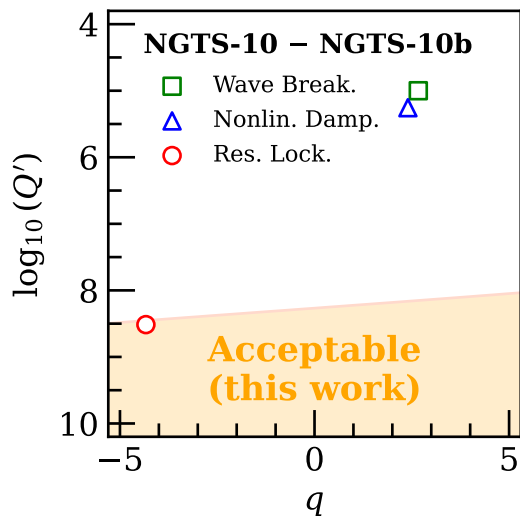
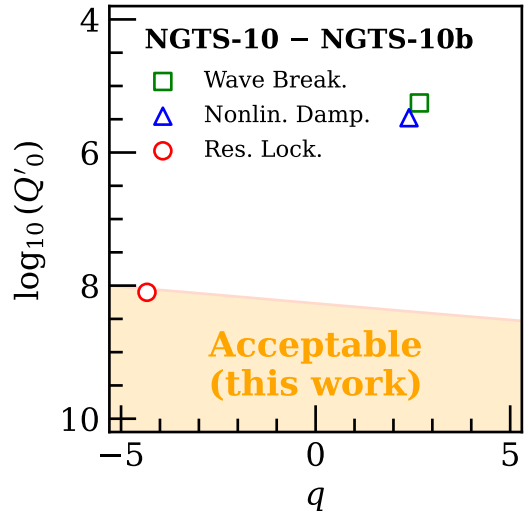


Figure 6. Acceptable condition (orange shaded region) in (q, Q'_0) (upper panel) and (q, Q') (lower panel) for the NGTS-10 system obtained from our method. While abscissae in both panels represent q in equation (10), ordinates in the upper and lower panel are $\log_{10}(Q'_0)$ and $\log_{10}(Q')$, respectively. For comparison, we also present theoretically predicted values of q and Q'_0 by the wave breaking model (Barker & Ogilvie 2010, the green square), the nonlinear wave damping model (Essick & Weinberg 2016, the blue triangle) and the resonance locking model (Ma & Fuller 2021, the red circle).

$\sqrt{I_s/(M_s R_s^2)}$ of the MESA calculation (see Appendix D). We fix $\alpha_{\text{mb}} = 1.5 \times 10^{31} \text{ erg}$ as already described in Section 2.3 (see also Appendix B).

4. CONSTRAINT OF Q' IN TARGET SYSTEM

Figure 6 shows the allowed region (orange shade) for the tidal quality factor obtained from the NGTS-10 system. We can derive the boundary, $Q'_{0,\text{lim}}(q)$, of the al-

lowed region for Q'_0 (top panel), following the procedure described in Section 2.3; we obtain the acceptable range as

$$\log_{10}(Q'_0) \geq 8.268 + 0.050q. \quad (12)$$

The constraint on Q' (bottom panel of Figure 6) is directly obtained from equations (12) by substituting $\omega_{\text{tide}}/2\pi = 2.48 \text{ d}^{-1}$ (Table 3) into equation (10):

$$\begin{aligned} \log_{10}(Q') &\geq 8.268 + \left[0.050 - \log\left(\frac{\omega_{\text{tide}}/2\pi}{2 \text{ d}^{-1}}\right) \right] q \quad (13) \\ &= 8.268 + \left[-0.045 - \log\left(\frac{\omega_{\text{tide}}/2\pi}{2.48 \text{ d}^{-1}}\right) \right] q. \end{aligned}$$

Here, we omit max in equation (10) for simplification (see also Figure 7). We note that this is consistent with a statistical result of $\log_{10}(Q') \simeq 8.26 \pm 0.14$, which was estimated from the relation between the planet/star mass ratio and the orbital separation of more than 200 systems with hot Jupiters, by assuming constant Q' (Collier Cameron & Jardine 2018). We discuss the ω_{tide} dependency of equation (13) in Section 5.2

Figure 6 also plots previous theoretical results based on the tidal interaction by the wave breaking mechanism (the green square; Barker & Ogilvie 2010), the non-linear damping mechanism (the blue triangle; Es-sick & Weinberg 2016), and the resonance locking (the red circle; Ma & Fuller 2021) (see Appendix C for detail). The tidal quality factors derived from the wave braking and non-linear damping mechanisms are more than a hundred times smaller than our lower bound; in other words, these mechanisms predict considerably strong tidal torque, compared with that constrained by the NGTS-10 system. This suggests that the tidal efficiencies of these mechanisms should be weakened in the system with a slow rotator and a close-in gaseous planet. On the other hand, the resonance locking mechanism appears to provide a consistent result with our constraint as this mechanism can quantitatively explain the current position of the NGTS-10 system. However, Ma & Fuller (2021) show that this mechanism may be unlikely to be effective in the system of a low-mass star and a Jovian planet (see also Appendix C). At the moment, we do not know any plausible explanation about the weak tide of this system (see Section 5.2 for detail).

Using the obtained constraint, we can discuss the orbital decay of NGTS-10 b. By substituting equations (6), (9) and (13) and the value of Table 3 into the timescale of orbital decay $t_{\text{decay}} \equiv (\text{d} \ln \Omega_{\text{orb}}/\text{d}t)^{-1}$, we

derive t_{decay} for NGTS-10 b as

$$\begin{aligned} t_{\text{decay}} &= \frac{4Q'}{27} \frac{1}{\Omega_{\text{orb}}} \left(\frac{M_s}{M_p} \right) \left[\frac{G(M_s + M_p)}{\Omega_{\text{orb}}^2 R_s^3} \right]^{5/3} \\ &\gtrsim 5.6 \times 10^{-0.045q} \text{ Gyr}. \end{aligned} \quad (14)$$

This large timescale indicates that NGTS-10 b has not significantly migrated inward by the tidal interaction in the past. Also, we can discuss the observability of a variation in the transit timing (see the last two paragraphs of Section 2.1.3). The shift of transit arrival time t_{shift} during the observational duration t_{dur} can be estimated to be $t_{\text{shift}} = t_{\text{dur}}^2/t_{\text{decay}}$ (Collier Cameron & Jardine 2018, see also Birkby et al. 2014)⁸. Then, from equation (14), we have

$$t_{\text{shift}} \lesssim 0.56 \times 10^{0.043q} \times \left(\frac{t_{\text{dur}}}{10 \text{ yr}} \right)^2 \text{ s}. \quad (15)$$

We note that this value is about ten times smaller than the previous estimate assuming $Q' = 2 \times 10^7$ (McCormac et al. 2020; Alvarado-Montes et al. 2021). Even with the current observational techniques, $t_{\text{shift}} \gtrsim 10 \text{ s}$ is required for detecting the shift (Maciejewski et al. 2022). Therefore, equation (15) indicates that the transit timing shift of NGTS-10 b is not detectable within a few decades. That is to say, our method presents a more stringent constraint than what could be obtained from observations of transit timing variations.

5. DISCUSSION

5.1. Validity of assumption

In our method to constrain the tidal quality factor, we employed several simplified treatments to leverage the mathematical robustness of the unstable manifold (Section 2). We here discuss the validity of the simplifications and associated errors.

5.1.1. Time-dependent stellar properties

The most significant simplification that would affect the results is the assumption that the stellar properties, apart from the rotation rate, remain constant over time. As briefly mentioned in the beginning of Section 2, a main sequence star generally expands with evolution as the mean molecular weight in the core increases. We are adopting the observed (current) radius of NGTS-10, which must be larger than the radius averaged over the time from the ZAMS to the current epoch; R_s in our

⁸ This expression is obtained from equation (27) in Collier Cameron & Jardine (2018), which is twice as large as that of equation (7) in Birkby et al. (2014).

analysis (Sections 2-4) is slightly overestimated. However, we found that the errors due to this deviation in R_s is small, because two counteracting effects are canceled each other out. First, the larger R_s increases the right-hand side of equation (11) by strengthening of tidal torque (equation 9). This gives a larger forbidden region for fixed Q' , and therefore, results in larger $Q'_{0,\text{lim}}$, namely a tighter constraint on tidal torque. Second, however, larger I_s , as a consequence of the larger R_s (see Appendix D for detailed calculation), decreases the right-hand side of equation (11). This effect, which is obviously opposite to the first one, leads to a looser constraint. Quantitatively, these two effects provide a similar level of errors $\lesssim 0.1$ dex with the opposite signs in equations (12) and (13) for stars with $M \leq 0.8 M_\odot$, whose radius expands by 5-10 percent. For the target star, NGTS-10, we found that these two effects give comparable errors in absolute magnitude. Hence, the deviation of the constraints in equations (12) and (13) is less than 0.1 dex from the constraints given by the treatment using time-dependent R_s and I_s . In contrast, in more massive stars with $M \geq 0.9 M_\odot$, the radius increases more than 20 percent, and hence, the obtained constraints are expected to include an uncertainty of one order of magnitude.

5.1.2. Wind torque

We should also remark on the treatment of the wind torque (Section 2.1.2); we have assumed the time-independent magnetic braking parameter, α_{mb} . This treatment is reasonable for the samples in Figure 5, including NGTS-10, because the constant α_{mb} well reproduces the trend for stars whose Rossby number is smaller than the solar value (Section 2.1.2). However, the effect of the weakened magnetic braking (van Saders et al. 2016) should be taken into account for slower rotators (Appendix A). As the reduced Γ_{wind} enlarges the forbidden region (see equation 11), we should include this effect when we apply our procedure to slow rotators with the Rossby number greater than the solar value (Figure 8 and Appendix A).

In addition, the bimodality of the spin rate distribution of low mass stars, which is called the ‘intermediate period gap’, has been reported as another mysteries in the spin-down evolution (McQuillan et al. 2013, 2014; Davenport 2017; Reinhold & Hekker 2020; Gordon et al. 2021; Lu et al. 2022). Since this bimodality is particularly evident in K and M-type stars with $T_{\text{eff}} \lesssim 4500 K$, NGTS-10, which has $T_{\text{eff}} = 4600 \pm 150 K$, is marginally subject to this effect. Yet, we consider that this effect is minor because a constant α_{mb} reproduces the spin-rate distribution of cluster members with $T_{\text{eff}} = 4600 \pm 150 K$

reasonably well (Fig. 9 in Appendix A). In contrast, when dealing with the cooler stars where this bimodality is prominent, we should modify the treatment of Γ_{wind} .

5.1.3. Initial condition

Another important assumption in our analysis is that the initial position of $(\Omega_{\text{orb,init}}, \Omega_{\text{spin,init}})$ needs to be located above the unstable manifold so that it is outside the forbidden region (Figure 3). A caveat is that the astrophysically reasonable initial condition, $\Omega_{\text{spin,init}}/2\pi \gtrsim 0.1 \text{ d}^{-1}$ and $\Omega_{\text{orb,init}}/2\pi \lesssim 2 \text{ d}^{-1}$ (Section 2.2), could break this requirement for strong tide, $Q' \lesssim 10^{6.5}$ (Figure 4). However, in that case, it is impossible to reach observed $\Omega_{\text{spin}}/2\pi \approx 0.05 \text{ d}^{-1}$, including NGTS-10, (Figure 5) from the reasonable initial value, $\Omega_{\text{spin,init}}/2\pi \gtrsim 0.1 \text{ d}^{-1}$ because Ω_{spin} is monotonically increasing along any trajectory below the unstable manifold in the phase space (Figure 4 and equation 11). Furthermore, the extremely weak tide expected from the NGTS-10 system (equation 12) is safely consistent with the assumption for the initial condition (see also Section 5.2). We note that the other objects plotted in Figure 5 also suggest a weak tide so that the initial condition is well outside the forbidden region; discussion on these objects will be summarized in the forthcoming paper.

5.1.4. Beyond Two-body system

The fundamental presumption of this paper is that we consider the isolated two-body system consisting of a star and a planet (see beginning of Section 2). However, when a third body is present, the evolution of the system will be altered by its gravity; a possible outcome of such three-body interaction is the high-eccentricity migration of a planet in the late evolutionary stage (cf. Masuda 2017). If the NGTS-10 system had undergone such drastic migration recently, it could be transiently located in the forbidden region of the $\Omega_{\text{orb}} - \Omega_{\text{spin}}$ plane; in this case, we cannot rule out strong tidal torque in the NGTS-10 system.

However, the probability of observing such a system is considered to be low because the timescale of orbital decay, t_{decay} (equation 14), is generally short in the presence of the strong tidal interaction. If we apply $Q' = 10^6$ as a moderately strong tidal torque to the NGTS-10 system, we obtain $t_{\text{decay}} \approx 30 \text{ Myr}$ from equation (14). This timescale is a tiny fraction of the inferred age of NGTS-10 order than 7 Gyr (McCormac et al. 2020); the probability of a recent three-body interaction in the NGTS-10 system would not be high.

5.2. Implication from obtained weak tide

From equation (13), we obtain the dependency of the lower limit of Q' , which corresponds to the right-hand

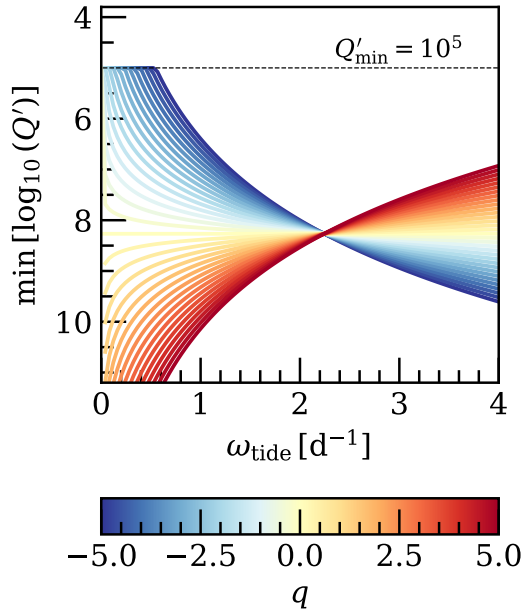


Figure 7. Behavior of the lower limit of tidal quality factor obtained from the NGTS-10 system, which is the right-hand side of equation (13), as a function of ω_{tide} for various q . The colors of lines represent the value of q , denoted by the bottom color-bar. We note that Q' is bounded by $Q' \geq Q'_{\min} = 10^5$, which is omitted in equation (13). $\omega_{\text{tide}} = 0 \text{ d}^{-1}$ corresponds to the completely synchronized case.

side of equation (13), on ω_{tide} and q in Figure 7. Supposing that the constraint derived from the NGTS-10 system can be extrapolated to synchronized systems with $\omega_{\text{tide}} \approx 0$, we verify the tidal properties for different q values in comparison to observed tendencies in synchronized systems on the basis of Figure 7.

Let us begin the discussion with the case of positive q , described by redder lines in Figure 7. In this case, the tidal torque is suppressed as a system approaches co-rotation ($\omega_{\text{tide}} = 0 \text{ d}^{-1}$). Then, the tidal interaction in a synchronized system, which satisfies $Q' \gtrsim 10^{8.5}$, is weak enough to be negligible. This tidal properties cannot explain observed synchronized systems with low inclination (e.g., Albrecht et al. 2012, 2022, see also Section 1). In order to solve this inconsistency, we should consider alternative tidal mechanisms, which work for a synchronized system effectively, in addition to the weak tidal interaction with $q > 0$ constrained by the NGTS-10 system. For example, the dynamical tide through the inertial wave is considered to be a possible mechanism (e.g., Mathis 2015).

On the other hand, the case of negative q , which is described by bluer lines in Figure 7, expects a strong tidal interaction in a synchronized system. Therefore, it is not necessary to consider additional effects in this case.

Examples of tidal mechanism with negative q include the resonance locking, which satisfies our constraint (Figure 6). Therefore, it can be a plausible tidal mechanism if further theoretical examination shows that the resonance locking mechanism is also valid for Jovian planets (see also Appendix C).

Long-term observations of the shift in transit timing (e.g., Ivshina & Winn 2022; Adams et al. 2024) are a powerful tool to pin down the constraint on the tidal interaction working in synchronized systems. Theoretical investigation with self-consistent numerical calculations (e.g., Ogilvie 2014) is also essential to elucidate the dominant tidal process operating in various types of two-body systems.

5.3. Extension to eccentric and misaligned systems

Our analysis has been restricted on planets in circular orbits on the co-planar plane with the stellar spin. An extension to close-in planets with finite eccentricity, e , and spin-orbit inclination angle, i , is meaningful because planets with large e or i have been identified with rate of 5-15 percent (Winn et al. 2010; Albrecht et al. 2012, 2022; Morgan et al. 2024). By employing formulations developed by previous works (Hut 1981; Eggleton et al. 1998; Ferraz-Mello et al. 2008; Barker & Ogilvie 2009; Xue et al. 2014), we can formulate AM co-evolution of eccentric and misaligned planets. We expect to obtain a forbidden region formed by a three dimensional unstable manifold in the four-dimensional phase space of $(\Omega_{\text{orb}}, \Omega_{\text{spin}}, e, i)$. In such a case, we should consider the tidal dissipation not only in the stellar interior but also in the planetary interior, both of which affect the shape of trajectories in the $(\Omega_{\text{orb}}, \Omega_{\text{spin}}, e, i)$ space (Jackson et al. 2008; Bonomo et al. 2017; Efroimsky & Makarov 2022). Therefore, the shape of the unstable manifolds with respect to the e and i directions is considered to depend on the efficiencies of these two tidal processes. A quantitative investigation of these dependencies is a subject for future work.

It should be noted that the unstable manifolds used in the current paper correspond to the projections of such general cases onto the two-dimensional plane at $e = 0$ and $i = 0$. Unstable manifolds for finite e and i projected onto that plane are different from the unstable manifold for $e = i = 0$. However, from the characteristic properties of the unstable manifold, the system evolves while ensuring that $(\Omega_{\text{orb}}, \Omega_{\text{spin}})$ remain outside the forbidden region determined by (e, i) at any given time. Therefore, provided that the system has $e = i = 0$ at the time of observation, we can safely use the forbidden region in Figure 2 to constrain the tidal torque, regard-

less of the evolutionary history of e and i (see Section 2.3).

5.4. Applications to different objects

Our framework can be directly applied to systems where the spin AM of the companion is negligible (Section 2.1). We argued that systems with large $\Omega_{\text{orb}}/\Omega_{\text{spin}}$ gives a strong constraint on Q' in Section 2.3. In addition to that, a more massive companion is preferred to provide a tighter constraint because $d\Omega_{\text{spin}}/d\Omega_{\text{orb}} \propto \mu \approx M_p$ (equation 11) so that a larger forbidden region is formed. This is the main reason why we used the massive Jovian planet, NGTS-10 b.

A promising candidate for such massive companions that readily comes to mind is a brown dwarf. An additional advantage of a brown dwarf around a low-mass star is that its formation is supposed to proceed simultaneously with that of the host star (see, e.g., Offner et al. 2023), which enables us to apply the initial conditions for planetary systems (Section 2.2) to brown-dwarf systems with a simple extrapolation. We expect the non-synchronized system with a low-mass star and a brown dwarf to provide a tight constraint of Q' even if $\Omega_{\text{orb}}/\Omega_{\text{spin}} (> 1)$ is relatively small. A caveat is that such systems may be rare firstly because the number of close-in brown dwarfs orbiting K-type stars is depleted compared to brown dwarfs orbiting other types of stars (Grieves et al. 2021) and secondly because a system with a close-in brown dwarf and an M-type star is easily synchronized owing to their small host-to-companion mass ratio.

We would like to mention the constraint inferred from exoplanetary systems with terrestrial planets because some of them have considerably large $\Omega_{\text{orb}}/\Omega_{\text{spin}}$. Unfortunately, however, even the system with the largest $\Omega_{\text{orb}}/\Omega_{\text{spin}} \simeq 100$ consisting of an M-type star and a terrestrial planet, KOI-4777 – KOI-4777 b (Cañas et al. 2022)⁹, gives only a weak constraint, $Q'_0 \gtrsim 10^5$, in comparison with the result obtained from the NGTS-10 system (equation 12). This is because the advantage of the large $\Omega_{\text{orb}}/\Omega_{\text{spin}}$ is overwhelmed by the disadvantage of the small M_p .

Compact stars, such as white dwarfs and neutron stars, are also good candidates. Although we have to modify the formulation to consider different formation paths to these objects and relativistic effects particularly for neutron stars, the fundamental concept regarding a forbidden region can be universally applied. However, we should note that it is difficult to observe a

non-synchronized system because most of close-in systems frequently observed as cataclysmic stars or X-ray binaries are considered to be synchronized ones (e.g., Mazeh 2008).

We can extend our framework to the non-synchronized binary consisting of two low-mass stars. For such a system, we should explicitly calculate the evolution of the rotation, $\Omega_{\text{spin},2}$, of the secondary star with magnetic braking, in addition to $\Omega_{\text{spin},1}$ of the primary star in the governing equations (e.g., Fleming et al. 2019). We can follow the same procedure using the two-dimensional unstable manifold in the three-dimensional phase space of $(\Omega_{\text{orb}}, \Omega_{\text{spin},1}, \Omega_{\text{spin},2})$ (cf. Section 5.3). Indeed, Lurie et al. (2017) reported several such systems in their compilation of eclipsing binaries detected by *Kepler*.

5.5. Magnetic star-planet interaction

It is considered that magnetic star-planet interaction also plays an important role in the evolution of the system (Cuntz et al. 2000). If a planetary orbit is located inside the Alfvén surface the sub-Alfvénic region of the stellar wind, the energy and angular momentum are transferred by the Alfvén wings scenario (Cohen et al. 2010; Strugarek et al. 2014), which is motivated by planet–satellite magnetic interactions in the solar system (Goldreich & Lynden-Bell 1969; Neubauer 1980, 1998). The torque produced by the magnetic interaction, Γ_{mag} , is formulated by numerical simulations (Strugarek 2016; Strugarek et al. 2017).

By formally replacing Γ_{tide} with $\Gamma_{\text{tide}} + \Gamma_{\text{mag}}$ in equation (11), we can extend our formalism. Ahuir et al. (2021) conducted comprehensive numerical simulations for the AM co-evolution in the star-planet system, including all $\Gamma_{\text{wind}}, \Gamma_{\text{tide}}$, and Γ_{mag} , and pointed out the forbidden region in the phase space of $(\Omega_{\text{orb}}, \Omega_{\text{spin}})$.

6. SUMMARY AND CONCLUSION

The aim of this paper is to construct a framework to obtain a robust constraint of the tidal Q' factor that is not subject to the indeterminacy of initial conditions and the uncertainty of stellar ages. For this purpose, we presented the method to restrict Q' from a single set of observed orbital rotation of a companion object and spin of a host object, $(\Omega_{\text{orb}}, \Omega_{\text{spin}})$, by utilizing the argument of dynamical system theory.

We first introduced the model to calculate the evolution of the AM of stellar spin and the AM of the orbital rotation of a planet under the time-independent stellar and planetary properties. The co-evolution of these AMs is governed by the tidal interaction between the star and the planet and the magnetic braking of the star through stellar winds. By tracking the AM

⁹ The mass of KOI-4777 b is not determined (Cañas et al. 2022); for this estimate, we assume an Earth mass.

co-evolution from the astrophysically reasonable initial condition, we found that a forbidden region appears in the lower-right part of the $\Omega_{\text{orb}} - \Omega_{\text{spin}}$ plane, regardless of its evolutionary history. On the basis of the dynamical system theory, we also presented that the forbidden region is formed by the unstable manifold that corresponds to the evolutionary track starting from the origin, $(\Omega_{\text{orb}}, \Omega_{\text{spin}}) = (0, 0)$. As the location and configuration of the unstable manifold are characterized by the strength of the tidal interaction, we proposed that a constraint of Q' is obtained by comparing the observed $(\Omega_{\text{orb}}, \Omega_{\text{spin}})$ of a single star-planet system with the forbidden region for given stellar and planetary parameters and magnetic-braking strength.

Our framework can provide a tight constraint on tidal interaction in a system composed of a slow rotator and a close-in Jovian planet. We demonstrated that NGTS-10 – NGTS-10 b, the system with the currently known largest $\Omega_{\text{orb}}/\Omega_{\text{spin}}$, only allows extremely weak tide, $Q' \gtrsim 10^8$. This constraint is in conflict with the Q' values predicted by the wave braking mechanism or the

nonlinear-damping mechanism. Among the currently known mechanisms, only the resonance locking is consistent with this constraint, although this mechanism may not be effectively working in Jovian planets (Ma & Fuller 2021). Additionally, our constraint predicts that the shift of transit timing due to the tidal interaction for this system is too small to detect with the current observational accuracy within a few decades.

Our result obtained from the NGTS-10 system required re-examination of the tidal interaction at least for non-synchronized systems. Also, our proposed framework has the potential to apply to various non-synchronized binary systems including low-mass stars.

ACKNOWLEDGEMENT

T.T. is supported by IGPEES, WINGS Program in the University of Tokyo and Research Fellowships for Young Scientists in JSPS (24KJ0605). T.K.S. is supported by Grants-in-Aid for Scientific Research from the MEXT/JSPS of Japan, 22H01263.

APPENDIX

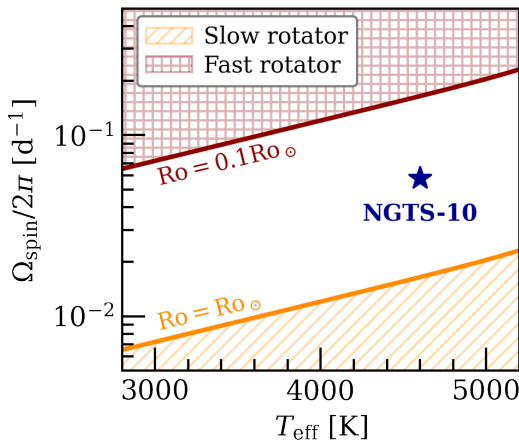


Figure 8. Fast-rotator ($Ro/Ro_{\odot} \leq 0.1$; red cross-hatched region) and slow-rotator ($Ro/Ro_{\odot} \geq 1$; orange diagonal-hatched region) regimes with the target star, NGTS-10 (star symbol), in T_{eff} (abscissa) - Ω_{spin} (ordinate) diagram. In order to calculate the Rossby number (equation A2), we adopt the model of Cranmer & Saar (2011) for $\tau_{\text{cz}}(T_{\text{eff}})$.

A. Γ_{WIND} FORMALISM

Theoretical models of magneto-rotator winds (e.g., Weber & Davis 1967; Sakurai 1985) give an approximated analytical expression for the wind torque,

$$\Gamma_{\text{wind}} \approx \dot{M} r_A \Omega_{\text{spin}}. \quad (\text{A1})$$

where \dot{M} is the mass-loss rate by the wind, and r_A expresses the Alfvén radius, which is the cylindrical radius where the radial components of the wind and local Alfvén velocities are equal. Given that \dot{M} and r_A depend on stellar parameters and rotational properties (e.g., Matt & Pudritz 2008; Cranmer & Saar 2011; Matt et al. 2012; Suzuki et al. 2013; Shoda et al. 2020), we can obtain the power-law relation between Γ_{wind} and Ω_{spin} (equation 8), leading to Skumanich’s law (equation 7).

Stellar rotational and magnetic activity can be characterized by Rossby number,

$$Ro \equiv \frac{2\pi}{\Omega_{\text{spin}} \tau_{\text{cz}}}, \quad (\text{A2})$$

where τ_{cz} is the convective turnover time (Noyes et al. 1984). Fast rotators generally correspond to young magnetically active stars. In this regime, Γ_{wind} does not rapidly increase with increasing Ω_{spin} but is shifted to the slow increase, $\Gamma_{\text{wind}} \propto \Omega_{\text{spin}}$, for $Ro/Ro_{\odot} \lesssim 0.1$ (equation 8; El-Badry et al. 2022; Gossage et al. 2023; Belloni et al. 2024), in accordance with the saturation of magnetic activity (Wright et al. 2011; Wheatley et al. 2018; See et al. 2019). In the slow-rotator regime, $Ro/Ro_{\odot} \gtrsim 1$, Γ_{wind} is more weakened than expected from the simple power-law dependence (van Saders et al. 2016; Hall et al. 2021; David et al. 2022; Metcalfe et al. 2022; Saunders et al. 2024), which has also been investigated theoretically (Metcalfe & van Saders 2017; Tokuno

Table 4. The list of clusters and their age we use.

Cluster	Age (Myr)	Ref. (Age)	Ref. (Ω_{spin} and T_{eff})
α Persei	80	1	1
Pleiades	125	2	2,3
M50	150	2	2,4
NGC 2516	150	2	2,5
Group X	300	6	6,7
NGC 3532	300	8	8
NGC 2281	450	9	9
M37	500	2	2,10
Preasepe	700	2	2,11
NGC 6811	950	2	2,12,13,14,15
NGC 6819	2500	16	16,17
Ruprecht 147	2700	17	17,18
M67	4000	19	19,20

References— 1. Boyle & Bouma (2023), 2. Godoy-Rivera et al. (2021), 3. Rebull et al. (2016), 4. Irwin et al. (2009), 5. Irwin et al. (2007), 6. Messina et al. (2022), 7. Newton et al. (2022), 8. Fritzewski et al. (2021), 9. Fritzewski et al. (2023), 10. Hartman et al. (2009), 11. Rebull et al. (2017), 12. Meibom et al. (2011), 13. Curtis et al. (2019), 14. Santos et al. (2019), 15. Santos et al. (2021), 16. Meibom et al. (2015), 17. Curtis et al. (2020), 18. Gruner & Barnes (2020), 19. Gruner et al. (2023), 20. Dungee et al. (2022).

et al. 2023). We do not consider the latter effect because our target star, NGTS-10, is still before entering the slow-rotator regime (Figure 8).

B. ESTIMATION OF α_{MB}

We are adopting $\alpha_{\text{mb}} = 1.5 \times 10^{31}$ erg as the reference value of the wind torque when $\Omega_{\text{spin}}/2\pi = 0.05 \text{ d}^{-1}$ for the target star, NGTS-10, which has $M_s = 0.70 M_\odot$. This value is determined to reproduce the observed spin-down trend of low-mass stars with similar mass. For this purpose, we use stars with $T_{\text{eff}} = 4600 \pm 150$ K in open clusters (Table 4). The MESA calculation shows the duration of the pre-MS before the ZAMS is ~ 100 Myr for the star with $M_s = 0.70 M_\odot$. Then, we select the clusters whose age is $\gtrsim 100$ Myr.

An advantage of using clusters is that the age of a cluster, which is derived from the isochrone fitting in a HR diagram combined with gyrochronology (e.g., Barnes 2003; Soderblom 2010), can be used as the reasonable estimate for the stellar age of the cluster members because they are considered to form simultaneously (e.g.,

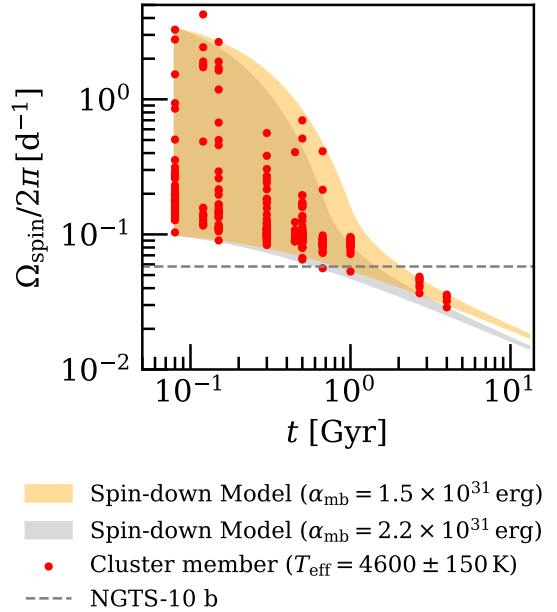


Figure 9. Comparison between observed spin rates, $\Omega_{\text{spin}}/2\pi$, of low-mass stars with $T_{\text{eff}} = 4600 \pm 150$ K in various open clusters (red circles) and the spin-down model result for $M_s = 0.7 M_\odot$ and $\alpha_{\text{mb}} = 1.5 \times 10^{31}$ erg (orange shaded region; our estimation) and 2.2×10^{31} erg (grey shaded region; Matt et al. 2015) against stellar age, t . We set the initial spin rates to cover the distribution of the stars in α Persei at $t = 80$ Myr. We also show the spin rate of NGTS-10 as the dashed horizontal line.

Soderblom 2010)¹⁰. Stellar spin rates can be measured from the periodic variation of light curves due to star spots (e.g. García et al. 2014; McQuillan et al. 2014). *Gaia* (Gaia Collaboration et al. 2018, 2023) provides the color magnitude to derive the effective temperature through the color- T_{eff} relation (Curtis et al. 2020)¹¹.

We calculate equation (5) with switching off tidal interaction, $\Gamma_{\text{tide}} = 0$, to derive the time evolution of Ω_{spin} from the initial values that encompass the range of the observed stellar spin rates, $0.1 \text{ d}^{-1} \leq \Omega_{\text{spin,init}}/2\pi \leq 3.3 \text{ d}^{-1}$, in α Persei, the youngest cluster with 80 Myr among our samples. We vary α_{mb} but fix the other parameters in Table 3 to determine the best-fit value of $\alpha_{\text{mb}} = 1.5 \times 10^{31}$ erg such that the model calculations with different $\Omega_{\text{spin,init}}$ cover the lower and upper envelopes of the observed distribution in the $t - \Omega_{\text{spin}}$ diagram (orange shaded region and red circles in Figure 9). This chosen value is moderately smaller than the

¹⁰ Some open clusters show multiple age populations (Cordoni et al. 2018), which may cause an error in the estimate of the stellar age.

¹¹ We assume the solar metallicity, which is roughly satisfied for our selected samples.

value, $\alpha_{\text{mb}} = 2.2 \times 10^{31}$ erg (gray shaded region), estimated from the scaling relation calibrated by the solar rotation (Matt et al. 2015). We consider that the deviation is likely due to newly obtained constraints from the cluster data with ages $\gtrsim 2.5$ Gyr (Curtis et al. 2020; Gruner & Barnes 2020; Dungee et al. 2022; Gruner et al. 2023, see also Figure 9).

C. THEORETICAL PREDICTION OF Q' FORMULATION

In this paper we did not specify the detailed physical mechanism of tidal interaction but used the general expression of the tidal quality factor, equation (10). We gave the general constraint, in comparison with the previous results based on the three different mechanisms, in Figure 6. We briefly introduce these mechanisms with the specific expressions regarding Q' below.

The first process is the wave braking mechanism (Barker & Ogilvie 2010, 2011): Large-amplitude internal gravity waves excite nonlinear oscillations, which damp the waves themselves and causes strong dissipation of the wave energy in the radiative core of a low-mass star. Barker & Ogilvie (2010) obtained

$$Q'_{\text{BO10}} \simeq 1 \times 10^5 \times \left(\frac{\mathcal{G}_s}{\mathcal{G}_\odot}\right)^{-1} \left(\frac{M_s}{M_\odot}\right)^2 \times \left(\frac{R_s}{R_\odot}\right) \left(\frac{\omega_{\text{tide}}/2\pi}{2.0 \text{ d}^{-1}}\right)^{-8/3}, \quad (\text{C3})$$

from their numerical simulations, where \mathcal{G}_s is a parameter that depends on the stellar structure. Equation (C3) gives $Q'_0 = 1.8 \times 10^5$ and $q = 8/3$ for NGTS-10 (green square in Figure 6), which yield $Q' = 1.0 \times 10^5$ listed in Barker (2020).

The second process is the nonlinear wave damping mechanisms: the numerical simulation conducted by Es-sick & Weinberg (2016) shows the nonlinear oscillation itself leads to energy dissipation through cascades, even in the absence of the wave breaking, in the system composed of a low-mass star and a hot Jupiter. They showed the tidal quality factor that is available for Jovian planets with $M_p \gtrsim 0.3 M_J$ as

$$Q'_{\text{EW16}} \simeq 2 \times 10^5 \times \left(\frac{M_p}{M_J}\right)^{1/2} \left(\frac{\omega_{\text{tide}}/2\pi}{2.0 \text{ d}^{-1}}\right)^{-2.4}, \quad (\text{C4})$$

providing $Q'_0 = 3.0 \times 10^5$ and $q = 2.4$ for NGTS-10 (blue circle in Figure 6).

The third process is the resonance locking mechanism, suggested by Fuller (2017). The energy dissipation by the tidal force is enhanced by the resonance between the tidal frequency and the stellar g-mode frequency. Ma &

Table 5. The setting of the MESA stellar evolution code.

Control name	Our setting	Ref.
Initial abundance	The solar metallicity	1
Reaction net work	“pp_and_cno_extras.net”	
Reaction rates	JINA REACLIB	2
Atmosphere	“Eddington”	
Mixing length	$\alpha_{\text{MLT}} = 2.0$	-
Diffusion	No	
Overshooting	No	
Mass Loss	No	

References—1. Grevesse & Sauval (1998), 2. Cyburt et al. (2010)

Fuller (2021) investigated the efficiency of this effect for a low-mass star and derived the tidal quality factor as

$$Q'_{\text{MF21}} \simeq 2 \times 10^6 \times \left(\frac{M_p}{M_J}\right) \left(\frac{M_s}{M_\odot}\right)^{-8/3} \left(\frac{R_s}{R_\odot}\right)^5 \times \left(\frac{t_\alpha}{5 \text{ Gyr}}\right) \left(\frac{\Omega_{\text{orb}}/2\pi}{0.5 \text{ d}^{-1}}\right)^{13/3}, \quad (\text{C5})$$

where t_α is the mode evolution timescale, which is determined by the stellar structure and evolution. We use $\Omega_{\text{orb}} \gg \Omega_{\text{spin}}$, namely, $\Omega_{\text{orb}} \approx \omega_{\text{tide}}/2$, when comparing with equation (10). It should be mentioned that the resonance locking may operate only for low-mass planets with $M_p \lesssim 0.1 M_J$ because the non-linear effects prevent the resonance (see Ma & Fuller 2021). In this paper, however, we assume this mechanism occurs on NGTS-10 b to give $Q'_0 = 1.3 \times 10^8$ and $q = -13/3$ (red circle in Figure 6)¹².

D. CALCULATION OF I_s

We determine I_s , which is assumed to be time-independent (Section 2), by using MESA stellar evolution code (r12278) with the input parameters summarized in Table 5¹³. To follow the evolution of NGTS-10, we calculate the time evolution of a $M_s = 0.7 M_\odot$ star from the ZAMS to 14 Gyr (\approx the age of the universe), which is before the end of the MS phase. Figure 10 presents the time variation of a dimensionless quantity, gyration radius, $\hat{r}_g \equiv \sqrt{I_s/(M_s R_s^2)}$ (cf. Damiani & Lanza 2015; Damiani & Díaz 2016). \hat{R}_g slowly decreases with time as the star evolves to core-halo-like structure. We are

¹² In Ma & Fuller (2021), Q'_0 for NGTS-10 was not explicitly presented. We used the stellar parameters for WASP-43, a star similar to NGTS-10, presented in their paper, to derive these values.

¹³ This setting reproduces the physical properties of the present Sun well. We upload the inlists in Zenodo: [10.5281/zenodo.8385153](https://zenodo.org/record/8385153)

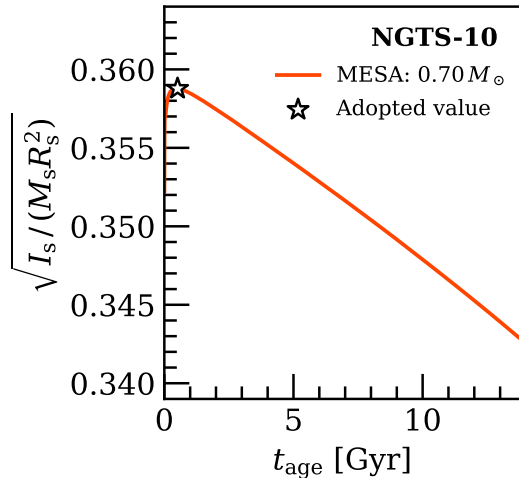


Figure 10. Time evolution of \hat{r}_g for $M_s = 0.7M_\odot$ computed by the MESA (the orange line). The star-shaped symbol represents the adopted value for the time-independent I_s in our calculations (see text for detail).

employing

$$I_s \equiv M_s R_s^2 \hat{r}_{g,\max}^2 \quad (\text{D6})$$

for our calculations, where $\hat{r}_{g,\max}^2$ is the maximum gyration radius shown by the star symbol in Figure 10.

Equation (D6) obviously overestimates I_s firstly because $\hat{r}_{g,\max}$ is larger than \hat{r}_g averaged over the evolution until the current time and secondly because R_s adopted from the observed value (Table 3) is also larger than the time averaged radius (Section 5.1). By this overestimate of I_s we can avoid overconstraining the tidal quality factor, as discussed in Section 5.1. The deviation of the constraint on Q' due to the overestimate is within $\lesssim 0.1$ dex with respect to the NGTS-10 system.

E. AUTONOMOUS SYSTEM

The theoretical background of this paper is based on the fact that the systems consisting of equations (3) and (4) can be treated as two-dimensional autonomous systems under some presumptions. In this section, we briefly introduce the proof of the property of the autonomous system used in Section 2.2 (e.g., Arnold 1992; Hsieh & Sibuya 1999, for detail).

We consider an n -dimensional autonomous system

$$\frac{d\mathbf{x}(t)}{dt} = \mathbf{f}(\mathbf{x}) \Leftrightarrow \begin{cases} \frac{dx_1(t)}{dt} = f_1(x_1, \dots, x_n) \\ \vdots \\ \frac{dx_n(t)}{dt} = f_n(x_1, \dots, x_n) \end{cases}, \quad (\text{E7})$$

where t , $x_i(t)$, and f_i (for $i = 1, \dots, N$) represent the time as the independent variable, the element of the Euclid space as a dependent variable, and the Lipschitz-continuous function whose arguments are x_i , respectively. For abbreviation, we use the vector notation $\mathbf{x} = (x_1, \dots, x_n)^T$ and $\mathbf{f}(\mathbf{x}) = (f_1(\mathbf{x}), \dots, f_n(\mathbf{x}))^T$, where ‘‘T’’ means transposition of a vector. At this time, the solution of equation (E7) is shown as the trajectory in the n -dimensional phase space of (x_1, \dots, x_n) . Then, we can deduce that the tangent vector of the trajectory is equal to $\mathbf{f}(\mathbf{x})$.

Here, let $\mathbf{x}_*(t)$ be the unique solution of the initial-value problem for equation (E7) when $\mathbf{x}(0) = \mathbf{x}_{\text{init}}$, where \mathbf{x}_{init} is a particular vector. In this case, $\mathbf{x}_*(t-t_0)$ for an arbitrarily selected time t_0 solves the initial-value problem for equation (E7) when $\mathbf{x}(t_0) = \mathbf{x}_{\text{init}}$. Therefore, we find that the trajectory in the phase space is determined independently of the value of t . Moreover, it indicates that two trajectories that pass through the same point are identical, which is equivalent to that two different trajectories have no intersection.

REFERENCES

- Adams, E. R., Jackson, B., Sicking, A. A., et al. 2024, arXiv e-prints, arXiv:2404.07339, doi: [10.48550/arXiv.2404.07339](https://doi.org/10.48550/arXiv.2404.07339)
- Ahuir, J., Strugarek, A., Brun, A. S., & Mathis, S. 2021, A&A, 650, A126, doi: [10.1051/0004-6361/202040173](https://doi.org/10.1051/0004-6361/202040173)
- Akeson, R. L., Chen, X., Ciardi, D., et al. 2013, PASP, 125, 989, doi: [10.1086/672273](https://doi.org/10.1086/672273)
- Albrecht, S., Winn, J. N., Johnson, J. A., et al. 2012, ApJ, 757, 18, doi: [10.1088/0004-637X/757/1/18](https://doi.org/10.1088/0004-637X/757/1/18)
- Albrecht, S. H., Dawson, R. I., & Winn, J. N. 2022, PASP, 134, 082001, doi: [10.1088/1538-3873/ac6c09](https://doi.org/10.1088/1538-3873/ac6c09)
- Alvarado-Montes, J. A., Sucerquia, M., García-Carmona, C., et al. 2021, MNRAS, 506, 2247, doi: [10.1093/mnras/stab1081](https://doi.org/10.1093/mnras/stab1081)
- Angus, R., Aigrain, S., Foreman-Mackey, D., & McQuillan, A. 2015, MNRAS, 450, 1787, doi: [10.1093/mnras/stv423](https://doi.org/10.1093/mnras/stv423)
- Arnold, V. I. 1992, Ordinary Differential Equations (Springer Science & Business Media)
- Baraffe, I., Homeier, D., Allard, F., & Chabrier, G. 2015, A&A, 577, A42, doi: [10.1051/0004-6361/201425481](https://doi.org/10.1051/0004-6361/201425481)
- Barker, A. J. 2020, MNRAS, 498, 2270, doi: [10.1093/mnras/staa2405](https://doi.org/10.1093/mnras/staa2405)

- Barker, A. J., & Ogilvie, G. I. 2009, *MNRAS*, 395, 2268, doi: [10.1111/j.1365-2966.2009.14694.x](https://doi.org/10.1111/j.1365-2966.2009.14694.x)
- . 2010, *MNRAS*, 404, 1849, doi: [10.1111/j.1365-2966.2010.16400.x](https://doi.org/10.1111/j.1365-2966.2010.16400.x)
- . 2011, *MNRAS*, 417, 745, doi: [10.1111/j.1365-2966.2011.19322.x](https://doi.org/10.1111/j.1365-2966.2011.19322.x)
- Barnes, S. A. 2003, *ApJ*, 586, 464, doi: [10.1086/367639](https://doi.org/10.1086/367639)
- . 2007, *ApJ*, 669, 1167, doi: [10.1086/519295](https://doi.org/10.1086/519295)
- Belloni, D., Schreiber, M. R., Moe, M., El-Badry, K., & Shen, K. J. 2024, *A&A*, 682, A33, doi: [10.1051/0004-6361/202347931](https://doi.org/10.1051/0004-6361/202347931)
- Benbakoura, M., Réville, V., Brun, A. S., Le Poncin-Lafitte, C., & Mathis, S. 2019, *A&A*, 621, A124, doi: [10.1051/0004-6361/201833314](https://doi.org/10.1051/0004-6361/201833314)
- Benomar, O., Bazot, M., Nielsen, M. B., et al. 2018, *Science*, 361, 1231, doi: [10.1126/science.aao6571](https://doi.org/10.1126/science.aao6571)
- Birkby, J. L., Cappetta, M., Cruz, P., et al. 2014, *MNRAS*, 440, 1470, doi: [10.1093/mnras/stu343](https://doi.org/10.1093/mnras/stu343)
- Bonomo, A. S., Desidera, S., Benatti, S., et al. 2017, *A&A*, 602, A107, doi: [10.1051/0004-6361/201629882](https://doi.org/10.1051/0004-6361/201629882)
- Borucki, W. J., Koch, D., Basri, G., et al. 2010, *Science*, 327, 977, doi: [10.1126/science.1185402](https://doi.org/10.1126/science.1185402)
- Bouvier, J., Forestini, M., & Allain, S. 1997, *A&A*, 326, 1023
- Boyle, A. W., & Bouma, L. G. 2023, *AJ*, 166, 14, doi: [10.3847/1538-3881/acd3e8](https://doi.org/10.3847/1538-3881/acd3e8)
- Cañas, C. I., Mahadevan, S., Cochran, W. D., et al. 2022, *AJ*, 163, 3, doi: [10.3847/1538-3881/ac3088](https://doi.org/10.3847/1538-3881/ac3088)
- Choi, J., Dotter, A., Conroy, C., et al. 2016, *ApJ*, 823, 102, doi: [10.3847/0004-637X/823/2/102](https://doi.org/10.3847/0004-637X/823/2/102)
- Cohen, O., Drake, J. J., Kashyap, V. L., Sokolov, I. V., & Gombosi, T. I. 2010, *ApJL*, 723, L64, doi: [10.1088/2041-8205/723/1/L64](https://doi.org/10.1088/2041-8205/723/1/L64)
- Collier Cameron, A., & Jardine, M. 2018, *MNRAS*, 476, 2542, doi: [10.1093/mnras/sty292](https://doi.org/10.1093/mnras/sty292)
- Collins, K. A., Kielkopf, J. F., & Stassun, K. G. 2017, *AJ*, 153, 78, doi: [10.3847/1538-3881/153/2/78](https://doi.org/10.3847/1538-3881/153/2/78)
- Cordoni, G., Milone, A. P., Marino, A. F., et al. 2018, *ApJ*, 869, 139, doi: [10.3847/1538-4357/aaedc1](https://doi.org/10.3847/1538-4357/aaedc1)
- Cranmer, S. R., & Saar, S. H. 2011, *ApJ*, 741, 54, doi: [10.1088/0004-637X/741/1/54](https://doi.org/10.1088/0004-637X/741/1/54)
- Cuntz, M., Saar, S. H., & Musielak, Z. E. 2000, *ApJL*, 533, L151, doi: [10.1086/312609](https://doi.org/10.1086/312609)
- Curtis, J. L., Agüeros, M. A., Douglas, S. T., & Meibom, S. 2019, *ApJ*, 879, 49, doi: [10.3847/1538-4357/ab2393](https://doi.org/10.3847/1538-4357/ab2393)
- Curtis, J. L., Agüeros, M. A., Matt, S. P., et al. 2020, *ApJ*, 904, 140, doi: [10.3847/1538-4357/abbf58](https://doi.org/10.3847/1538-4357/abbf58)
- Cyburt, R. H., Amthor, A. M., Ferguson, R., et al. 2010, *ApJS*, 189, 240, doi: [10.1088/0067-0049/189/1/240](https://doi.org/10.1088/0067-0049/189/1/240)
- Damiani, C., & Díaz, R. F. 2016, *A&A*, 589, A55, doi: [10.1051/0004-6361/201527100](https://doi.org/10.1051/0004-6361/201527100)
- Damiani, C., & Lanza, A. F. 2015, *A&A*, 574, A39, doi: [10.1051/0004-6361/201424318](https://doi.org/10.1051/0004-6361/201424318)
- Darwin, G. H. 1880, *Philosophical Transactions of the Royal Society of London Series I*, 171, 713
- Davenport, J. R. A. 2017, *ApJ*, 835, 16, doi: [10.3847/1538-4357/835/1/16](https://doi.org/10.3847/1538-4357/835/1/16)
- David, T. J., Angus, R., Curtis, J. L., et al. 2022, *ApJ*, 933, 114, doi: [10.3847/1538-4357/ac6dd3](https://doi.org/10.3847/1538-4357/ac6dd3)
- Davoudi, F., Baştürk, Ö., Yalçınkaya, S., Esmer, E. M., & Safari, H. 2021, *AJ*, 162, 210, doi: [10.3847/1538-3881/ac1baf](https://doi.org/10.3847/1538-3881/ac1baf)
- Dawson, R. I., & Johnson, J. A. 2018, *ARA&A*, 56, 175, doi: [10.1146/annurev-astro-081817-051853](https://doi.org/10.1146/annurev-astro-081817-051853)
- Dobbs-Dixon, I., Lin, D. N. C., & Mardling, R. A. 2004, *ApJ*, 610, 464, doi: [10.1086/421510](https://doi.org/10.1086/421510)
- Drażkowska, J., Bitsch, B., Lambrechts, M., et al. 2023, in *Astronomical Society of the Pacific Conference Series*, Vol. 534, *Protostars and Planets VII*, ed. S. Inutsuka, Y. Aikawa, T. Muto, K. Tomida, & M. Tamura, 717, doi: [10.48550/arXiv.2203.09759](https://doi.org/10.48550/arXiv.2203.09759)
- Dunee, R., van Saders, J., Gaidos, E., et al. 2022, *ApJ*, 938, 118, doi: [10.3847/1538-4357/ac90be](https://doi.org/10.3847/1538-4357/ac90be)
- Efroimsky, M., & Makarov, V. V. 2022, *Universe*, 8, 211, doi: [10.3390/universe8040211](https://doi.org/10.3390/universe8040211)
- Eggleton, P. P., Kiseleva, L. G., & Hut, P. 1998, *ApJ*, 499, 853, doi: [10.1086/305670](https://doi.org/10.1086/305670)
- El-Badry, K., Conroy, C., Fuller, J., et al. 2022, *MNRAS*, 517, 4916, doi: [10.1093/mnras/stac2945](https://doi.org/10.1093/mnras/stac2945)
- Esposito, M., Covino, E., Desidera, S., et al. 2017, *A&A*, 601, A53, doi: [10.1051/0004-6361/201629720](https://doi.org/10.1051/0004-6361/201629720)
- Essick, R., & Weinberg, N. N. 2016, *ApJ*, 816, 18, doi: [10.3847/0004-637X/816/1/18](https://doi.org/10.3847/0004-637X/816/1/18)
- Ferraz-Mello, S., Rodríguez, A., & Hussmann, H. 2008, *Celestial Mechanics and Dynamical Astronomy*, 101, 171, doi: [10.1007/s10569-008-9133-x](https://doi.org/10.1007/s10569-008-9133-x)
- Fleming, D. P., Barnes, R., Davenport, J. R. A., & Luger, R. 2019, *ApJ*, 881, 88, doi: [10.3847/1538-4357/ab2ed2](https://doi.org/10.3847/1538-4357/ab2ed2)
- Fortney, J. J., Dawson, R. I., & Komacek, T. D. 2021, *Journal of Geophysical Research (Planets)*, 126, e06629, doi: [10.1029/2020JE006629](https://doi.org/10.1029/2020JE006629)
- Fritzewski, D. J., Barnes, S. A., James, D. J., & Strassmeier, K. G. 2021, *A&A*, 652, A60, doi: [10.1051/0004-6361/202140894](https://doi.org/10.1051/0004-6361/202140894)
- Fritzewski, D. J., Barnes, S. A., Weingrill, J., et al. 2023, *A&A*, 674, A152, doi: [10.1051/0004-6361/202346083](https://doi.org/10.1051/0004-6361/202346083)
- Fuller, J. 2017, *MNRAS*, 472, 1538, doi: [10.1093/mnras/stx2135](https://doi.org/10.1093/mnras/stx2135)

- Gaia Collaboration, Brown, A. G. A., Vallenari, A., et al. 2018, *A&A*, 616, A1, doi: [10.1051/0004-6361/201833051](https://doi.org/10.1051/0004-6361/201833051)
- Gaia Collaboration, Vallenari, A., Brown, A. G. A., et al. 2023, *A&A*, 674, A1, doi: [10.1051/0004-6361/202243940](https://doi.org/10.1051/0004-6361/202243940)
- Gallet, F., & Bouvier, J. 2013, *A&A*, 556, A36, doi: [10.1051/0004-6361/201321302](https://doi.org/10.1051/0004-6361/201321302)
- . 2015, *A&A*, 577, A98, doi: [10.1051/0004-6361/201525660](https://doi.org/10.1051/0004-6361/201525660)
- Gallet, F., & Delorme, P. 2019, *A&A*, 626, A120, doi: [10.1051/0004-6361/201834898](https://doi.org/10.1051/0004-6361/201834898)
- García, R. A., Ceillier, T., Salabert, D., et al. 2014, *A&A*, 572, A34, doi: [10.1051/0004-6361/201423888](https://doi.org/10.1051/0004-6361/201423888)
- Godoy-Rivera, D., Pinsonneault, M. H., & Rebull, L. M. 2021, *ApJS*, 257, 46, doi: [10.3847/1538-4365/ac2058](https://doi.org/10.3847/1538-4365/ac2058)
- Goldreich, P., & Lynden-Bell, D. 1969, *ApJ*, 156, 59, doi: [10.1086/149947](https://doi.org/10.1086/149947)
- Goldreich, P., & Soter, S. 1966, *Icarus*, 5, 375, doi: [10.1016/0019-1035\(66\)90051-0](https://doi.org/10.1016/0019-1035(66)90051-0)
- Goodman, J., & Dickson, E. S. 1998, *ApJ*, 507, 938, doi: [10.1086/306348](https://doi.org/10.1086/306348)
- Gordon, T. A., Davenport, J. R. A., Angus, R., et al. 2021, *ApJ*, 913, 70, doi: [10.3847/1538-4357/abf63e](https://doi.org/10.3847/1538-4357/abf63e)
- Gossage, S., Kalogera, V., & Sun, M. 2023, *ApJ*, 950, 27, doi: [10.3847/1538-4357/acc86e](https://doi.org/10.3847/1538-4357/acc86e)
- Grevesse, N., & Sauval, A. J. 1998, *SSRv*, 85, 161, doi: [10.1023/A:1005161325181](https://doi.org/10.1023/A:1005161325181)
- Grieves, N., Bouchy, F., Lendl, M., et al. 2021, *A&A*, 652, A127, doi: [10.1051/0004-6361/202141145](https://doi.org/10.1051/0004-6361/202141145)
- Gruner, D., & Barnes, S. A. 2020, *A&A*, 644, A16, doi: [10.1051/0004-6361/202038984](https://doi.org/10.1051/0004-6361/202038984)
- Gruner, D., Barnes, S. A., & Weingrill, J. 2023, *A&A*, 672, A159, doi: [10.1051/0004-6361/202345942](https://doi.org/10.1051/0004-6361/202345942)
- Guillot, T., Burrows, A., Hubbard, W. B., Lunine, J. I., & Saumon, D. 1996, *ApJL*, 459, L35, doi: [10.1086/309935](https://doi.org/10.1086/309935)
- Hall, O. J., Davies, G. R., van Saders, J., et al. 2021, *Nature Astronomy*, 5, 707, doi: [10.1038/s41550-021-01335-x](https://doi.org/10.1038/s41550-021-01335-x)
- Harre, J. V., Smith, A. M. S., Barros, S. C. C., et al. 2023, *A&A*, 669, A124, doi: [10.1051/0004-6361/202244529](https://doi.org/10.1051/0004-6361/202244529)
- Hartman, J. D., Gaudi, B. S., Pinsonneault, M. H., et al. 2009, *ApJ*, 691, 342, doi: [10.1088/0004-637X/691/1/342](https://doi.org/10.1088/0004-637X/691/1/342)
- Hsieh, P.-F., & Sibuya, Y. 1999, *Basic theory of ordinary differential equations* (Springer Science & Business Media)
- Hut, P. 1981, *A&A*, 99, 126
- Irwin, J., Aigrain, S., Bouvier, J., et al. 2009, *MNRAS*, 392, 1456, doi: [10.1111/j.1365-2966.2008.14158.x](https://doi.org/10.1111/j.1365-2966.2008.14158.x)
- Irwin, J., Hodgkin, S., Aigrain, S., et al. 2007, *MNRAS*, 377, 741, doi: [10.1111/j.1365-2966.2007.11640.x](https://doi.org/10.1111/j.1365-2966.2007.11640.x)
- Ivshina, E. S., & Winn, J. N. 2022, *ApJS*, 259, 62, doi: [10.3847/1538-4365/ac545b](https://doi.org/10.3847/1538-4365/ac545b)
- Jackson, B., Greenberg, R., & Barnes, R. 2008, *ApJ*, 678, 1396, doi: [10.1086/529187](https://doi.org/10.1086/529187)
- Jontof-Hutter, D. 2019, *Annual Review of Earth and Planetary Sciences*, 47, 141, doi: [10.1146/annurev-earth-053018-060352](https://doi.org/10.1146/annurev-earth-053018-060352)
- Kawaler, S. D. 1988, *ApJ*, 333, 236, doi: [10.1086/166740](https://doi.org/10.1086/166740)
- Kunitomo, M., Suzuki, T. K., & Inutsuka, S.-i. 2020, *MNRAS*, 492, 3849, doi: [10.1093/mnras/staa087](https://doi.org/10.1093/mnras/staa087)
- Kurokawa, H., & Nakamoto, T. 2014, *ApJ*, 783, 54, doi: [10.1088/0004-637X/783/1/54](https://doi.org/10.1088/0004-637X/783/1/54)
- Lu, Y. L., Curtis, J. L., Angus, R., David, T. J., & Hattori, S. 2022, *AJ*, 164, 251, doi: [10.3847/1538-3881/ac9bee](https://doi.org/10.3847/1538-3881/ac9bee)
- Lurie, J. C., Vyhmeister, K., Hawley, S. L., et al. 2017, *AJ*, 154, 250, doi: [10.3847/1538-3881/aa974d](https://doi.org/10.3847/1538-3881/aa974d)
- Ma, L., & Fuller, J. 2021, *ApJ*, 918, 16, doi: [10.3847/1538-4357/ac088e](https://doi.org/10.3847/1538-4357/ac088e)
- Maciejewski, G., Knutson, H. A., Howard, A. W., et al. 2020, *AcA*, 70, 1, doi: [10.32023/0001-5237/70.1.1](https://doi.org/10.32023/0001-5237/70.1.1)
- Maciejewski, G., Fernández, M., Aceituno, F., et al. 2018, *AcA*, 68, 371, doi: [10.32023/0001-5237/68.4.4](https://doi.org/10.32023/0001-5237/68.4.4)
- Maciejewski, G., Fernández, M., Sota, A., et al. 2022, *A&A*, 667, A127, doi: [10.1051/0004-6361/202244280](https://doi.org/10.1051/0004-6361/202244280)
- Mannaday, V. K., Thakur, P., Southworth, J., et al. 2022, *AJ*, 164, 198, doi: [10.3847/1538-3881/ac91c2](https://doi.org/10.3847/1538-3881/ac91c2)
- Masuda, K. 2017, *AJ*, 154, 64, doi: [10.3847/1538-3881/aa7aeb](https://doi.org/10.3847/1538-3881/aa7aeb)
- Mathis, S. 2015, *A&A*, 580, L3, doi: [10.1051/0004-6361/201526472](https://doi.org/10.1051/0004-6361/201526472)
- Mathis, S., Auclair-Desrotour, P., Guenel, M., Gallet, F., & Le Poncin-Lafitte, C. 2016, *A&A*, 592, A33, doi: [10.1051/0004-6361/201527545](https://doi.org/10.1051/0004-6361/201527545)
- Matsumura, S., Peale, S. J., & Rasio, F. A. 2010, *ApJ*, 725, 1995, doi: [10.1088/0004-637X/725/2/1995](https://doi.org/10.1088/0004-637X/725/2/1995)
- Matsumura, S., Takeda, G., & Rasio, F. A. 2008, *ApJL*, 686, L29, doi: [10.1086/592818](https://doi.org/10.1086/592818)
- Matt, S., & Pudritz, R. E. 2008, *ApJ*, 681, 391, doi: [10.1086/587453](https://doi.org/10.1086/587453)
- Matt, S. P., Brun, A. S., Baraffe, I., Bouvier, J., & Chabrier, G. 2015, *ApJL*, 799, L23, doi: [10.1088/2041-8205/799/2/L23](https://doi.org/10.1088/2041-8205/799/2/L23)
- Matt, S. P., MacGregor, K. B., Pinsonneault, M. H., & Greene, T. P. 2012, *ApJL*, 754, L26, doi: [10.1088/2041-8205/754/2/L26](https://doi.org/10.1088/2041-8205/754/2/L26)
- Mayor, M., & Queloz, D. 1995, *Nature*, 378, 355, doi: [10.1038/378355a0](https://doi.org/10.1038/378355a0)
- Mazeh, T. 2008, in *EAS Publications Series*, Vol. 29, *EAS Publications Series*, ed. M. J. Goupil & J. P. Zahn, 1–65, doi: [10.1051/eas:0829001](https://doi.org/10.1051/eas:0829001)
- McCormac, J., Gillen, E., Jackman, J. A. G., et al. 2020, *MNRAS*, 493, 126, doi: [10.1093/mnras/staa115](https://doi.org/10.1093/mnras/staa115)

- McQuillan, A., Aigrain, S., & Mazeh, T. 2013, *MNRAS*, 432, 1203, doi: [10.1093/mnras/stt536](https://doi.org/10.1093/mnras/stt536)
- McQuillan, A., Mazeh, T., & Aigrain, S. 2014, *ApJS*, 211, 24, doi: [10.1088/0067-0049/211/2/24](https://doi.org/10.1088/0067-0049/211/2/24)
- Meibom, S., Barnes, S. A., Platais, I., et al. 2015, *Nature*, 517, 589, doi: [10.1038/nature14118](https://doi.org/10.1038/nature14118)
- Meibom, S., Barnes, S. A., Latham, D. W., et al. 2011, *ApJL*, 733, L9, doi: [10.1088/2041-8205/733/1/L9](https://doi.org/10.1088/2041-8205/733/1/L9)
- Messina, S., Nardiello, D., Desidera, S., et al. 2022, *A&A*, 657, L3, doi: [10.1051/0004-6361/202142276](https://doi.org/10.1051/0004-6361/202142276)
- Metcalf, T. S., & van Saders, J. 2017, *SoPh*, 292, 126, doi: [10.1007/s11207-017-1157-5](https://doi.org/10.1007/s11207-017-1157-5)
- Metcalf, T. S., Finley, A. J., Kochukhov, O., et al. 2022, *ApJL*, 933, L17, doi: [10.3847/2041-8213/ac794d](https://doi.org/10.3847/2041-8213/ac794d)
- Metcalf, T. S., Strassmeier, K. G., Ilyin, I. V., et al. 2023, *ApJL*, 948, L6, doi: [10.3847/2041-8213/acce38](https://doi.org/10.3847/2041-8213/acce38)
- Miotello, A., Kamp, I., Birnstiel, T., Cleves, L. C., & Kataoka, A. 2023, in *Astronomical Society of the Pacific Conference Series*, Vol. 534, *Protostars and Planets VII*, ed. S. Inutsuka, Y. Aikawa, T. Muto, K. Tomida, & M. Tamura, 501, doi: [10.48550/arXiv.2203.09818](https://doi.org/10.48550/arXiv.2203.09818)
- Morgan, M., Bowler, B. P., Tran, Q. H., et al. 2024, *AJ*, 167, 48, doi: [10.3847/1538-3881/ad0728](https://doi.org/10.3847/1538-3881/ad0728)
- Murray, C. D., & Dermott, S. F. 1999, *Solar system dynamics* (Cambridge University Press)
- Neubauer, F. M. 1980, *J. Geophys. Res.*, 85, 1171, doi: [10.1029/JA085iA03p01171](https://doi.org/10.1029/JA085iA03p01171)
- . 1998, *J. Geophys. Res.*, 103, 19843, doi: [10.1029/97JE03370](https://doi.org/10.1029/97JE03370)
- Newton, E. R., Rampalli, R., Kraus, A. L., et al. 2022, *AJ*, 164, 115, doi: [10.3847/1538-3881/ac8154](https://doi.org/10.3847/1538-3881/ac8154)
- Noyes, R. W., Weiss, N. O., & Vaughan, A. H. 1984, *ApJ*, 287, 769, doi: [10.1086/162735](https://doi.org/10.1086/162735)
- Offner, S. S. R., Moe, M., Kratter, K. M., et al. 2023, in *Astronomical Society of the Pacific Conference Series*, Vol. 534, *Protostars and Planets VII*, ed. S. Inutsuka, Y. Aikawa, T. Muto, K. Tomida, & M. Tamura, 275, doi: [10.48550/arXiv.2203.10066](https://doi.org/10.48550/arXiv.2203.10066)
- Ogilvie, G. I. 2013, *MNRAS*, 429, 613, doi: [10.1093/mnras/sts362](https://doi.org/10.1093/mnras/sts362)
- . 2014, *ARA&A*, 52, 171, doi: [10.1146/annurev-astro-081913-035941](https://doi.org/10.1146/annurev-astro-081913-035941)
- Ogilvie, G. I., & Lin, D. N. C. 2007, *ApJ*, 661, 1180, doi: [10.1086/515435](https://doi.org/10.1086/515435)
- Owen, J. E. 2019, *Annual Review of Earth and Planetary Sciences*, 47, 67, doi: [10.1146/annurev-earth-053018-060246](https://doi.org/10.1146/annurev-earth-053018-060246)
- Patra, K. C., Winn, J. N., Holman, M. J., et al. 2020, *AJ*, 159, 150, doi: [10.3847/1538-3881/ab7374](https://doi.org/10.3847/1538-3881/ab7374)
- Paxton, B., Bildsten, L., Dotter, A., et al. 2011, *ApJS*, 192, 3, doi: [10.1088/0067-0049/192/1/3](https://doi.org/10.1088/0067-0049/192/1/3)
- Paxton, B., Cantiello, M., Arras, P., et al. 2013, *ApJS*, 208, 4, doi: [10.1088/0067-0049/208/1/4](https://doi.org/10.1088/0067-0049/208/1/4)
- Paxton, B., Marchant, P., Schwab, J., et al. 2015, *ApJS*, 220, 15, doi: [10.1088/0067-0049/220/1/15](https://doi.org/10.1088/0067-0049/220/1/15)
- Paxton, B., Schwab, J., Bauer, E. B., et al. 2018, *ApJS*, 234, 34, doi: [10.3847/1538-4365/aaa5a8](https://doi.org/10.3847/1538-4365/aaa5a8)
- Paxton, B., Smolec, R., Schwab, J., et al. 2019, *ApJS*, 243, 10, doi: [10.3847/1538-4365/ab2241](https://doi.org/10.3847/1538-4365/ab2241)
- Penev, K., Bouma, L. G., Winn, J. N., & Hartman, J. D. 2018, *AJ*, 155, 165, doi: [10.3847/1538-3881/aaaf71](https://doi.org/10.3847/1538-3881/aaaf71)
- Penev, K., Zhang, M., & Jackson, B. 2014, *PASP*, 126, 553, doi: [10.1086/677042](https://doi.org/10.1086/677042)
- Perryman, M. 2018, *The Exoplanet Handbook* (Cambridge University Press)
- Rebull, L. M., Stauffer, J. R., Hillenbrand, L. A., et al. 2017, *ApJ*, 839, 92, doi: [10.3847/1538-4357/aa6aa4](https://doi.org/10.3847/1538-4357/aa6aa4)
- Rebull, L. M., Stauffer, J. R., Bouvier, J., et al. 2016, *AJ*, 152, 113, doi: [10.3847/0004-6256/152/5/113](https://doi.org/10.3847/0004-6256/152/5/113)
- Reinhold, T., & Hekker, S. 2020, *A&A*, 635, A43, doi: [10.1051/0004-6361/201936887](https://doi.org/10.1051/0004-6361/201936887)
- Remus, F., Mathis, S., & Zahn, J. P. 2012, *A&A*, 544, A132, doi: [10.1051/0004-6361/201118160](https://doi.org/10.1051/0004-6361/201118160)
- Ribas, Á., Bouy, H., & Merín, B. 2015, *A&A*, 576, A52, doi: [10.1051/0004-6361/201424846](https://doi.org/10.1051/0004-6361/201424846)
- Ricker, G. R., Winn, J. N., Vanderspek, R., et al. 2014, *Society of Photo-Optical Instrumentation Engineers (SPIE) Conference Series*, Vol. 9143, *Transiting Exoplanet Survey Satellite (TESS)* (Society of Photo-Optical Instrumentation Engineers (SPIE) Conference Series), 914320
- Rosário, N. M., Barros, S. C. C., Demangeon, O. D. S., & Santos, N. C. 2022, *A&A*, 668, A114, doi: [10.1051/0004-6361/202244513](https://doi.org/10.1051/0004-6361/202244513)
- Sakurai, T. 1985, *A&A*, 152, 121
- Santos, A. R. G., Breton, S. N., Mathur, S., & García, R. A. 2021, *ApJS*, 255, 17, doi: [10.3847/1538-4365/ac033f](https://doi.org/10.3847/1538-4365/ac033f)
- Santos, A. R. G., García, R. A., Mathur, S., et al. 2019, *ApJS*, 244, 21, doi: [10.3847/1538-4365/ab3b56](https://doi.org/10.3847/1538-4365/ab3b56)
- Saunders, N., van Saders, J. L., Lyttle, A. J., et al. 2024, *ApJ*, 962, 138, doi: [10.3847/1538-4357/ad1516](https://doi.org/10.3847/1538-4357/ad1516)
- Schou, J., Antia, H. M., Basu, S., et al. 1998, *ApJ*, 505, 390, doi: [10.1086/306146](https://doi.org/10.1086/306146)
- See, V., Matt, S. P., Folsom, C. P., et al. 2019, *ApJ*, 876, 118, doi: [10.3847/1538-4357/ab1096](https://doi.org/10.3847/1538-4357/ab1096)
- Shoda, M., Suzuki, T. K., Matt, S. P., et al. 2020, *ApJ*, 896, 123, doi: [10.3847/1538-4357/ab94bf](https://doi.org/10.3847/1538-4357/ab94bf)
- Skumanich, A. 1972, *ApJ*, 171, 565, doi: [10.1086/151310](https://doi.org/10.1086/151310)

- Soderblom, D. R. 2010, *ARA&A*, 48, 581,
doi: [10.1146/annurev-astro-081309-130806](https://doi.org/10.1146/annurev-astro-081309-130806)
- Strugarek, A. 2016, *ApJ*, 833, 140,
doi: [10.3847/1538-4357/833/2/140](https://doi.org/10.3847/1538-4357/833/2/140)
- Strugarek, A., Bolmont, E., Mathis, S., et al. 2017, *ApJL*, 847, L16, doi: [10.3847/2041-8213/aa8d70](https://doi.org/10.3847/2041-8213/aa8d70)
- Strugarek, A., Brun, A. S., Matt, S. P., & Réville, V. 2014, *ApJ*, 795, 86, doi: [10.1088/0004-637X/795/1/86](https://doi.org/10.1088/0004-637X/795/1/86)
- Suzuki, T. K., Imada, S., Kataoka, R., et al. 2013, *PASJ*, 65, 98, doi: [10.1093/pasj/65.5.98](https://doi.org/10.1093/pasj/65.5.98)
- Tayar, J., Claytor, Z. R., Huber, D., & van Saders, J. 2022, *ApJ*, 927, 31, doi: [10.3847/1538-4357/ac4bbc](https://doi.org/10.3847/1538-4357/ac4bbc)
- Tejada Arevalo, R. A., Winn, J. N., & Anderson, K. R. 2021, *ApJ*, 919, 138, doi: [10.3847/1538-4357/ac1429](https://doi.org/10.3847/1538-4357/ac1429)
- Tokuno, T., Suzuki, T. K., & Shoda, M. 2023, *MNRAS*, 520, 418, doi: [10.1093/mnras/stad103](https://doi.org/10.1093/mnras/stad103)
- Turner, J. D., Ridden-Harper, A., & Jayawardhana, R. 2021, *AJ*, 161, 72, doi: [10.3847/1538-3881/abd178](https://doi.org/10.3847/1538-3881/abd178)
- van Saders, J. L., Ceillier, T., Metcalfe, T. S., et al. 2016, *Nature*, 529, 181, doi: [10.1038/nature16168](https://doi.org/10.1038/nature16168)
- Weber, E. J., & Davis, Leverett, J. 1967, *ApJ*, 148, 217,
doi: [10.1086/149138](https://doi.org/10.1086/149138)
- Wheatley, P. J., West, R. G., Goad, M. R., et al. 2018, *MNRAS*, 475, 4476, doi: [10.1093/mnras/stx2836](https://doi.org/10.1093/mnras/stx2836)
- Winn, J. N., Fabrycky, D., Albrecht, S., & Johnson, J. A. 2010, *ApJL*, 718, L145,
doi: [10.1088/2041-8205/718/2/L145](https://doi.org/10.1088/2041-8205/718/2/L145)
- Winn, J. N., & Fabrycky, D. C. 2015, *ARA&A*, 53, 409,
doi: [10.1146/annurev-astro-082214-122246](https://doi.org/10.1146/annurev-astro-082214-122246)
- Wong, I., Shporer, A., Vissapragada, S., et al. 2022, *AJ*, 163, 175, doi: [10.3847/1538-3881/ac5680](https://doi.org/10.3847/1538-3881/ac5680)
- Wright, N. J., Drake, J. J., Mamajek, E. E., & Henry, G. W. 2011, *ApJ*, 743, 48,
doi: [10.1088/0004-637X/743/1/48](https://doi.org/10.1088/0004-637X/743/1/48)
- Xue, Y., Suto, Y., Taruya, A., et al. 2014, *ApJ*, 784, 66,
doi: [10.1088/0004-637X/784/1/66](https://doi.org/10.1088/0004-637X/784/1/66)
- Yee, S. W., Winn, J. N., Knutson, H. A., et al. 2020, *ApJL*, 888, L5, doi: [10.3847/2041-8213/ab5c16](https://doi.org/10.3847/2041-8213/ab5c16)
- Zahn, J. P. 1966, *Annales d'Astrophysique*, 29, 489
- . 1975, *A&A*, 41, 329
- . 1977, *A&A*, 57, 383
- Zahn, J. P., & Bouchet, L. 1989, *A&A*, 223, 112